date10 May 2020

Droplet dynamics on viscoelastic soft substrate: towards coalescence control

Fong Yew Leong[1, a)] and Duc Vinh Le[1]
*A*STAR Institute of High Performance Computing, 1 Fusionopolis Way, Connexis, Singapore 138632*

We study the dynamical behavior of droplets on a viscoelastic soft substrate. Using thin film approximation for hydrodynamics and time-dependent Winkler's substrate model, we show numerically how droplet growth depends strongly on viscous damping characteristic of the substrate, leading to asymmetric stick-slip dynamics corroborated by experimental observations. Scaling arguments are presented to rationalize radial growth and the underlying substrate response to viscoelastic limits. Using an adjacent pair of inflating droplets, we report strongly diverse coalescence outcomes with non-linear coalescence times, including attraction, repulsion, and remarkably, a separation regime, within which the two droplets grows away from each other and remain separated due to intervening wetting ridges. Together, our results indicate strong interactions between substrate and droplet across viscoelastic and capillary time-scales, with practical implications for smart surface engineering, condensation and coalescence control.

I. INTRODUCTION

The wetting behavior of liquid droplet[1] on a soft substrate has been a subject of significant interest[2–4] with numerous practical applications.[5,6] Unlike a rigid substrate, a soft substrate deforms in response to the unbalanced vertical force component at the contact line of the liquid, leading to a microscopic surface protrusion commonly known as a wetting ridge.[7] The corollary to this observation is that the well-known Young's law is inaccurate for droplet behavior on soft substrates.[8] To this, one could introduce a Neumann's triangle to resolve the forces at the contact line[9] of a droplet on soft solids[10] or deformable membranes.[11] This approach, however, fails to account for elastic nature of the substrate near the contact line[12] and also neglects liquid-vapor thermodynamic equilibrium.[13]

The latter raises the question on the effects of disjoining pressures[14] near the contact line, which can be considered under the form of an adsorbed precursor film whose thickness is defined by a balance of stresses including the Laplace pressure.[15] To that, Ahmed and co-workers[16] considered a sessile droplet on a thin film, whose thickness is defined by disjoining and capillary pressures. In turn, the liquid film rests on a soft substrate defined only by a Winkler's stress model,[17] which directly relates an imposed stress to substrate deformation. The result is a thermodynamically consistent model which can be used to describe droplet behavior on soft substrates, such as one involving contact angle hysteresis[18] or simply an elastic substrate that can be modeled accurately using the finite elements method.[19] Unfortunately, the thin film model is typically compromised by the lack of detail of the deformable substrate itself, which tends to be complex,[20] even without accounting for large strain phenomena such as the Shuttleworth effect.[21]

So far we have focused mainly on static droplets on soft substrates, but what about a droplet in motion? For one, a droplet can be induced to move along stiffness gradients on substrates generally from stiffer regions to less stiff ones,[22] although for non-wetting droplets with large contact angles, the opposite may be true.[23] Interestingly, such spontaneous motions of droplets are reminiscent of durotactic migration of biological cells on substrates with similar stiffness gradients.[24]

Alternatively, a stationary droplet on a soft substrate can be made to grow in volume so that the contact line moves outwards as the droplet expands. Accordingly, Kajiya and co-workers[25] found that as a droplet is inflated on a soft SBS-paraffin gel, there exists a stick-slip regime at some intermediate growth rate, where the contact line is pinned momentarily and suddenly slips forward. This stick-slip regime bridges the continuous advancing regime at low and high growth rates, which suggests a coupling of visco-elastic frequency of the soft material and the contact line velocity.[26] A separate experiment using a dip coating approach also yields similar stick-slip transitions from continuous regimes,[27] but without further theoretical developments, the nature of these dynamic transitions remain elusive.

On a related note, perhaps the most common occurrence of droplet growth in nature lies in the form of water condensation on a cool surface. Sokuler and co-workers[28] found that the coalescence between growing condensed droplets seems to occur more slowly on soft substrates compared to hard ones, which suggests a link between soft substrates and coalescence. Understandably, the coalescence of drops has been a subject of innumerable works,[29,30] but for sessile drops, one refers to contact line dynamics,[31] including asymmetric drops[32] and exceptional surface forces[33] leading to coalescence. Unfortunately, a survey of the literature[34] shows that studies on coalescence are mainly focused on the development of capillary bridge, and few in the way of the substrate playing any significant role in the process.

Notably, Karpitschka and co-workers[35] slid two droplets down a soft gel and observed between the pair of droplets either attraction or repulsion, the repulsion part being coined the 'inverse Cheerios effect', which is the opposite of the name-sake phenomena of cereals sticking to each other or to the walls of a breakfast bowl.[36] The authors had categorized their findings as, drop-wise attraction on a thick substrate, and

a)Electronic mail: leongfy@ihpc.a-star.edu.sg

drop-wise repulsion on a thin substrate. To that, they proposed a geometric mechanism based on the substrate thickness, but not its viscoelasticity.

On that note, some recent developments in engineering soft materials[37] herald new possibilities in tailoring viscoelastic smart substrates to specific damping characteristics. Such viscoelastic substrates could interact with droplets across dynamical time-scales with precision, leading to non-intrusive droplet manipulation at interfacial scales and therefore exciting new technologies that has not been explored hitherto.

In this study, we are interested in exploring droplet behavior on thin films subjected to disjoining pressures on a hypothetical viscoelastic substrate through numerical modeling. Using thin film approximations, we show how the growth of an inflating droplet could either be smoothly continuous, or stick-slip depending on the substrate viscoelasticity. This dynamical analysis is extended to the case of two inflating droplets so that coalescence could occur between them, and we rationalize the diverse patterns that emerge as a consequence.

II. THEORY AND MODELING

Consider a liquid droplet on a soft deformable substrate covered by an equilibrium thin film (Fig. 1a). Using the long wave approximation,[38] the thickness of the liquid film h evolves in two-dimensional space x, y and time t, according to

$$\partial_t h = -\frac{1}{3\mu}\nabla h^3 \nabla P - G, \tag{1}$$

where μ is the dynamic viscosity and G is the source term. The excess pressure P, a Lagrange multiplier, depends on h_s the deviation of the substrate height from the far-field equilibrium, so that

$$\gamma\nabla^2(h+h_s)+\Pi(h)=P, \tag{2}$$

$$\gamma_s\nabla^2 h_s - \Pi(h) = -\left(P+P_s\right), \tag{3}$$

where γ and γ_s are the liquid-vapor and solid-liquid interfacial tensions.

The disjoining stress due to solid-liquid interaction is modeled as a sum of short-ranged repulsive and long ranged attractive forces per area, as

$$\Pi(h) = \Pi_0\left[\left(\frac{h_e}{h}\right)^n - \left(\frac{h_e}{h}\right)^m\right], \tag{4}$$

where Π_0 is a constant, h_e is the equilibrium film thickness and (n,m) are positive exponents chosen as (3,4).[38,39] Truncated linear[40] or layered[18] models are reasonable choices as well, even if the derivative of the disjoining pressure function may be discontinuous. The use of disjoining pressure caters to a continuous thin liquid film which resolves issues related to the three phase contact line.

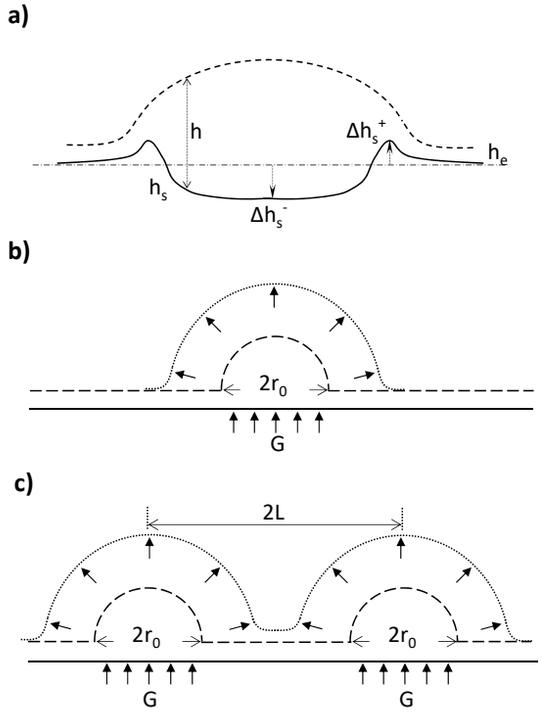

FIG. 1. (a) Schematic diagram of droplet on soft substrates, where h is liquid height, h_s is substrate deformation and h_e is equilibrium film thickness. (b) Single droplet with initial radius r_0 (dashed) growing at rate G into a larger droplet (dotted) at time t (see Section III). (c) Two identical droplets, initially spaced $2L$ apart (dashed), each growing at rate G until coalescence at time t_c along with the formation of a transient capillary bridge (dotted) between them (see Section IV).

The underlying soft substrate responds to the hydrodynamic and disjoining stress through mechanical deformation. Assuming linear elasticity, we employ the Winkler's foundation model,[17] which linearly associates local deformation to applied local stress,[16,40] and include a dynamic term to account for dynamic viscoelasticity,[41] so that

$$P_s = k_s h_s + \mu_s \partial_t h_s, \tag{5}$$

where k_s is the coefficient of subgrade reaction, or substrate stiffness coefficient, and μ_s is the viscous damping coefficient.

The evolution equation 1 is initialized with a droplet of hemispherical cap of specific radius and numerical solutions are performed on a finite element solver (Comsol v3.5a) and mesh independence is verified in each case to within 5 % accuracy of all dependent variables. For water, the room temperature bulk value for surface tension γ is 0.072 $N\cdot m^{-1}$ and dynamic viscosity is 0.001 $Pa\cdot s$. The equilibrium film thickness h_e is set as 0.10 μm, which is reasonably small for simulation scales larger than a micron. The disjoining pressure coefficient Π_0 is 5.0 MPa, a value found to yield an equilib-

rium droplet size close to its initial state of a hemispherical cap of specific radius, which makes it convenient for initialization and subsequent parametric analyses.

Although the thin film approximation, $\partial(h+h_s)/\partial x_i \ll 1$ and $\partial h_s/\partial x_i \ll 1$ for $x_i = x, y$, may not be strictly valid throughout the computational domain, it has been shown to adequately describe droplets with $O(1)$ aspect ratios[16], and compare well against other slip models[42] and experiments[39]. The present model yields droplet morphology and dynamic behavior that matches experimental observations (see Section III).

III. DROPLET GROWTH

Here we investigate the dynamic growth of a droplet initialized as a hemispherical cap of radius $r_0 \equiv 10h_e$ at a constant "inflation" rate[25] defined by a growth rate of film height G within a circle of radius r_0 (Fig. 1b). Here we assume that the infusion process is non-intrusive with growth rates fast compared to evaporation rates, and the droplets are sufficiently small for elasto-capillary waves and surface tension gradients to be negligible.

Following parameter calibration (see Appendix A), the model substrate has a reference stiffness k_{ref} of 6.94×10^{-5} and tension γ_{ref} of 0.52. Simulations are conducted varying the substrate viscous damping, normalized and referred to as $3G\mu_s h_e/4\gamma$.

We report in Fig. 2 droplet and substrate height profiles taken at a normalized growth time $3Gt/2r_0$ of 150 and the effect of viscous damping $3G\mu_s h_e/4\gamma$ from 10^0 to 10^4. First we observe that the substrate deformation magnitudes decrease with increasing viscous damping, with minimum value indicating the depth of deformation at the center of the drop, and maximum value indicating the height of the wetting ridge. Also, we find that the characteristics of substrate growth are distinctive in each case, starting from the smooth symmetric growth profile (I), to an asymmetric one (II), to one characterized by stick-slip motion of the growing drop, evidenced by residual ridge patterns (III), which becomes increasingly uni-directional in growth (IV), and finally back to a smooth symmetric growth (V).

These observations agree with the trends reported in droplet growth experiments which also feature transitions from continuous to stick-slip and back to continuous growth profiles.[25,26] In addition, we note that the residual patterns left on the substrate after droplet growth experiments[25] differs greatly from their proposed concentric ring model, which suggests stick-slip growth in all directions. In reality, the ridge patterns progress by propping outwards in directional periodic steps that give rise to a clear advancing edge. On the other end of the droplet, there exists a trailing edge which hardly moved at all. We find that these features are well captured by our model and the substrate pattern at the stick-slip regime (see case III) closely matches the image obtained by Kajiya et al.[25] Apart from ridge patterns, we also found that the wetting ridge is taller along the trailing edge compared to the advancing front (see cases II to IV). This creates a physical barrier against slip at the trailing edge and further reinforces the directionality of drop spreading at the front.

As for symmetry breaking, we point out that asymmetric solutions emerge due to numerical imperfections of the finite element mesh scheme, and these solutions are otherwise spontaneous and stable (see Appendix B). Parallel tests based on alternative mesh schemes set up using non-interactive internal boundaries, results in nearly identical solutions for all cases involving symmetry breaking (II to IV), each only differing in the direction of droplet spreading.

Here we further analyze droplet growth behavior based on viscous damping. Given that the initial droplet height based on a hemispherical droplet cap is $h_0 \equiv 10h_e$, we define the droplet within a continuous boundary with a height threshold equal to twice the equilibrium film thickness $h > 2h_e$. This yields the droplet area $A_{h>2h_e}$ as a function of time t, for a given constant growth rate of film height G within a circle of radius r_0. Figure 3 shows a plot of apparent droplet radius $r \equiv \sqrt{A_{h>2h_e}/\pi}$ against normalized time $3Gt/2r_0$ for varying substrate viscous damping $3G\mu_s h_e/4\gamma$. Based on an idealized hemispherical droplet cap of radius r and volume $V = 2\pi r^3/3$, initialized at radius r_0, the radial growth expression can be written as,

$$\left(\frac{r}{r_0}\right)^3 = \frac{3Gt}{2r_0} + 1, \tag{6}$$

which is shown to produce a good fit for the undamped ($\mu_s = 0$) case (see inset of Fig. 3). Indeed, this one-third power law for radial growth rate $r \sim t^{1/3}$ is frequently found in condensation of droplets.[43] However, for soft substrates, smaller droplets find significant fractions of their volume buried deep within the substrate due to large Laplace pressures. Balancing capillary and substrate pressures $\gamma\nabla^2 h \sim k_s h_s$ leads to $h \sim r^2$, so given the volume of a half ellipsoid $V \sim r^2 h$, one expects a one-fourth power law $r \sim t^{1/4}$ for radial growth for small droplets, which is indeed the case as shown in inset of Fig. 3a. Note that this should not be confused with diffusion-limited condensation growth, which incidentally also features a one-fourth power law.[44]

On the other hand, excessive viscous damping $3G\mu_s h_e/4\gamma$ leads to a decoupling between the droplet and the substrate, resulting in a droplet with a greater surface area $A_{h>2h_e}$ compared to an under-damped droplet of the same volume. In this case, we could use a generalized drop model of volume $V = \pi h(3r^2 + h^2)/6$, with height h and initial radius r_0, and express the radial growth as

$$\left(\frac{r}{r_0}\right)^3 = \left(\frac{4}{a^3 + 3a}\right)\left(\frac{3Gt}{2r_0}\right) + 1, \tag{7}$$

where $a \equiv h/r$ is a constant ratio of droplet height to radius; naturally, $a = 1$ leads to the spherical cap limit. By inspection, we find that $a \sim 0.64$ yields an excellent approximation for the over-damped limit (Fig. 3a).

Further inspection shows that both under-damped ($\mu_s = 0$) and over-damped radial growth profiles are bridged by a tran-

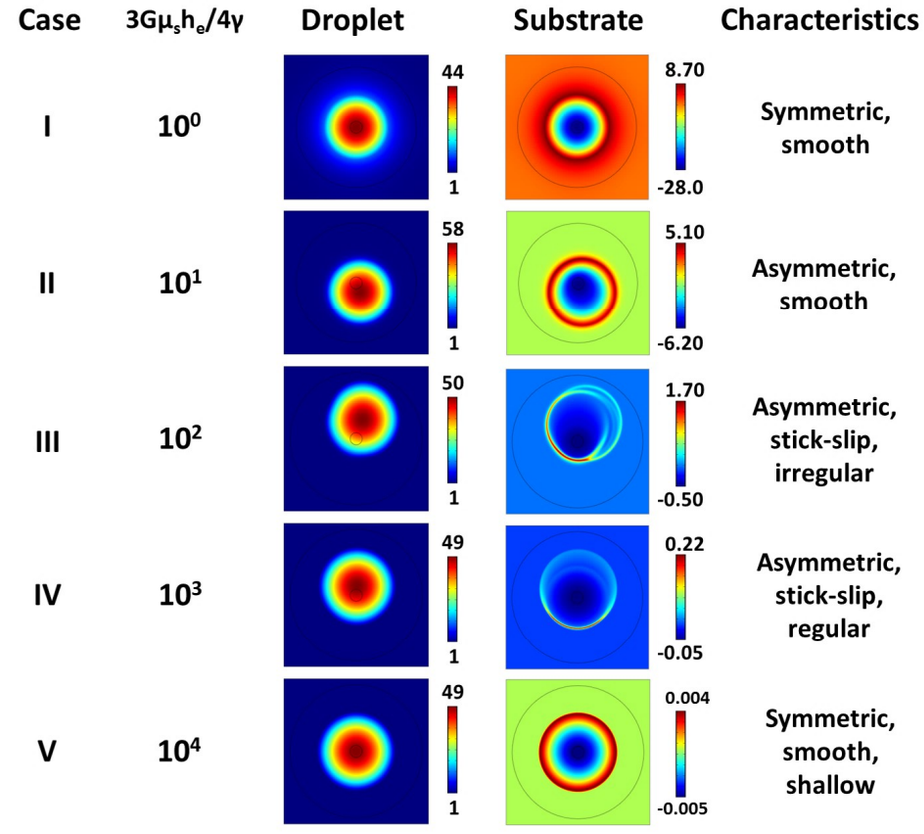

FIG. 2. Snapshot of an inflating droplet initialized as a hemispherical cap of radius $r_0 \equiv 10h_e$ taken at normalized time $3Gt/2r_0$ of 150, on a substrate with stiffness k_{ref} of 6.94×10^{-5} and tension γ_{ref} of 0.52. Results are shown in panels of size 250 by 250 and color-scaled to height. Cases I to V (top down) characterize substrate response to increasing viscous damping $3G\mu_s h_e/4\gamma$ from 10^0 to 10^4, leading to continuous to stick-slip to continuous transitions as reported in experiments.[26]

sition case II (plus symbol) and a stick-slip case III (star symbol). Specifically, the latter stick-slip regime (case III) features a staggered growth curve (in asterisk symbols), where its deviations become increasingly pronounced at larger drop sizes. To see stick-slip dynamics in detail, we plot the time evolution of a case III droplet along an arbitrary lateral axis, with droplet height shown on top (shifted vertically for clarity) and substrate height below (Fig. 3b). For comparison, we scale the substrate height against film thickness h_e, and droplet height against the droplet length scale $r_0 \equiv 10h_e$, and with that, one finds that the positions of substrate wetting ridges are aligned with the slowed sections of the moving contact time, as the droplet undergoes stick-slip motion to the right. On the left, however, the wetting ridge walls up rapidly in time, which directly prevents the droplet from slipping in that direction. Droplet-substrate time-series plotted along different axes also result in qualitatively similar trends (results not shown).

To see how droplet and substrate dynamics depends on growth rates, we plot the substrate height for both maximum wetting ridge height (positive values) and minimum depression depth (negative values) against viscous damping $3G\mu_s h_e/4\gamma$ (cases I to V), and show that the height differences taken at time $3Gt/2r_0$ of 150 all decay to zero with increasing viscous damping $3G\mu_s h_e/4\gamma$ (Fig. 4a). Holding the normalized time $3Gt/2r_0$ constant at 150, we show that varying growth rates $3G\mu/4\gamma$ over two orders of magnitude results in a collapse into the same master curve, thus demonstrating that the droplet and substrate heights are appropriately normalized and they are independent of growth rates.

Using the same approach, we check for parametric sensitivity for static solutions in terms of substrate stiffness k_s and tension γ_s. Figure 4b shows logarithmic plots of the maximum wetting ridge height $|\Delta h_s^+|/h_e$ and depression $|\Delta h_s^-|/h_e$ against substrate stiffness $k_s h_e^2/\gamma$, varying tension γ_s/γ all taken at time $3Gt/2r_0$ of 150. Qualitatively, we find that the center depression magnitude $|\Delta h_s^-|$ decays monotonically with increasing substrate stiffness k_s, whereas the wetting ridge height $|\Delta h_s^+|$ is at maximum for some intermediate stiffness, and diminishes in both limits of substrate stiffness. Another observation is that the wetting ridge height is greater than depression depth $|\Delta h_s^+| > |\Delta h_s^-|$ in the stiff limit and that the reverse $|\Delta h_s^-| > |\Delta h_s^+|$ is true in the soft limit, with a crossover at, again, some intermediate stiffness. This conforms to the macroscopic intuition that droplets tend to sink in soft substrates and float on stiff ones.

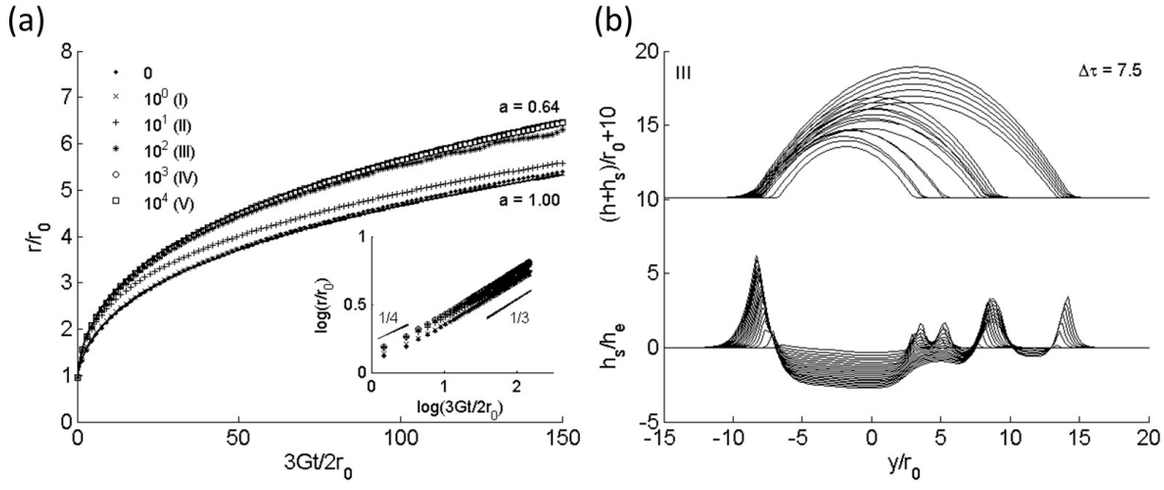

FIG. 3. (a) Radial growth of droplet initialized as a hemispherical cap of radius $h_0 \equiv 10h_e$ on substrate in time $3Gt/2r_0$ with viscous damping $3G\mu_s h_e/4\gamma$ corresponding to cases I to V (see legend). Distinct under-damped ($\mu_s = 0$) and over-damped radial growth profiles are bridged by a transition case II (plus symbol) and a stick-slip case III (star symbol). Continuous line plots refer to an idealized spherical cap growth (a = 1) and a generalized growth model (a = 0.64), where $a \equiv h/r$ is the height to radius ratio. Inset shows log-log re-plot revealing a transition from a 1/4 power law for small droplets to 1/3 expected for constant volumetric growth. (b) Stick-slip dynamics of a droplet (top) and substrate (bottom) height profiles under the stick-slip regime (case III) along an arbitrary axis. Droplet height profiles (top) are shifted vertically by plus 10 units for clarity and the frame interval $3G\Delta t/2r_0$ is 7.5 units. Here, the wetting ridge on the left is shown to wall up significantly as the droplet undergoes periodic stick-slip motion towards the right.

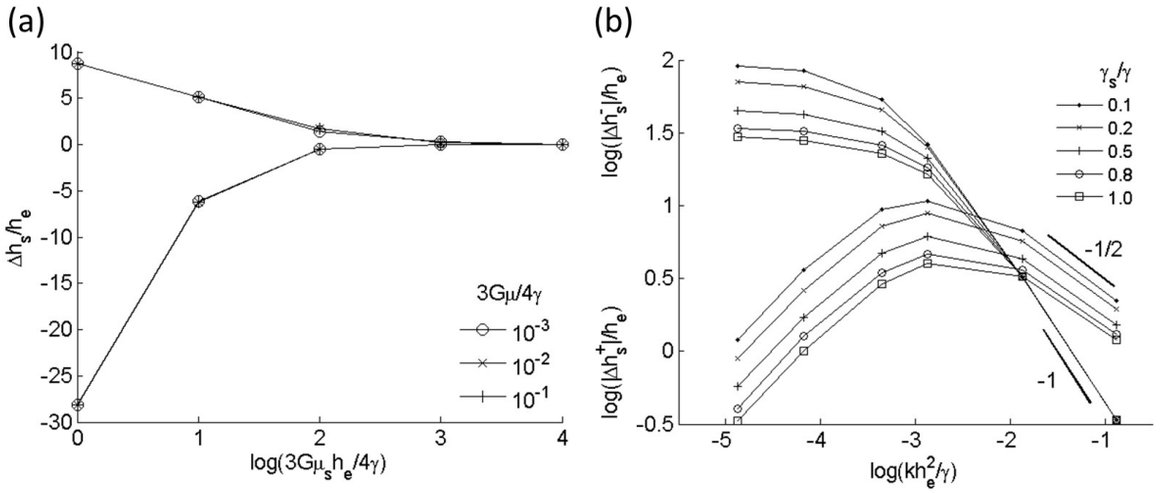

FIG. 4. (a) Maximum wetting ridge height (positive values) and minimum depression depth (negative values) decay with viscous damping $3G\mu_s h_e/4\gamma$ (cases I to V) taken at time $3Gt/2r_0$ of 150. Results are independent of growth rate, as shown by the collapse of data under different growth rates (see legend). (b) Logarithmic plots of maximum wetting ridge height $|\Delta h_s^+|/h_e$ and depression $|\Delta h_s^-|/h_e$ against substrate stiffness $k_s h_e^2/\gamma$, varying tension γ_s/γ, taken at time $3Gt/2r_0$ of 150.

In the limit of stiff substrates, the bulk of the droplet rests above the equilibrium substrate height. Balancing substrate rigidity and capillarity at droplet center, $k_s\Delta h_s^- \sim \gamma/R$, leads to a scaling argument for depression magnitude $|\Delta h_s^-$ at the drop center, namely,

$$\frac{\Delta h_s^-}{h_e} \sim \frac{h_e}{R}\left(\frac{k_s h_e^2}{\gamma}\right)^{-1}. \tag{8}$$

For a drop at a constant volume, the power law for the depression magnitude Δh_s^- scaling against stiffness parameter $k_s h_e^2/\gamma$ is -1 as indicated by the slope shown in Fig. 4b. Note that this scaling argument is independent of substrate tension γ_s, and one indeed finds that the various Δh_s^- curves with different tensions collapse into a master curve towards the stiff limit.

As for contact line elevation Δh_s^+ in the stiff limit, one considers the lateral length-scale $l^2 \sim \gamma_s/k_s$, so the balance of substrate rigidity and capillarity across the ridge yields $k_s\Delta h_s^+ \sim \gamma/l$ and leads to

$$\frac{\Delta h_s^+}{h_e} \sim \left[\left(\frac{k_s h_e^2}{\gamma}\right)\left(\frac{\gamma_s}{\gamma}\right)\right]^{-\frac{1}{2}}. \tag{9}$$

Note the ridge elevation Δh_s^+ scales inversely against stiffness parameter $k_s h_e^2/\gamma$ to the power of one-half, matched by the sloped line in Fig. 4b. Note the same inverse square-root dependence on substrate tension γ_s, a trend also corroborated by numerical data (see legend of Fig. 4b).

IV. DROPLET COALESCENCE

Here we extend the preceding growth analysis to two droplets simultaneously inflated at a constant rate G within a circle of radius r_0 centered at a distance $2L_c \equiv 10r_0$ from each other and investigate coalescence phenomena in time as the distance between the contact lines diminish to zero (Fig. 1c). At this distance, droplets are sufficiently close that they interact with each other through substrate coupling, so spreading is no longer determined by stochastic symmetry breaking (Fig. 2).

Figure 5 shows the evolution of substrate due to both droplet growth and coalescence, in terms of viscous damping $3G\mu_s h_e/4\gamma$. We observe a surprisingly rich diversity in substrate patterns due to non-linear coalescence outcomes, as we traverse top-down with increasing viscous damping as before (cases I to V). Case I is characterized by late coalescence between the substrate ring ridges, and the maximum ridge heights can be found equidistant between the individual droplet centers. Case II, in contrast to case I, is characterized by an early coalescence, so that the coalesced substrate resembles an elongated depression at the center surrounded by a ridge, which are raised at the far ends away from the center. Case III, like case II, is also characterized by early coalescence, but in addition, overlapping and intersecting substrate residual patterns are observed as expected of growth under the stick-slip regime.

Remarkably, case IV shows no coalescence and the droplets remain separated, even up to $3Gt/2r_0$ of 150. Instead, the droplets grow independently and extend in the direction away from each other. Note also that the ridges between the droplets are raised into a physical barrier between the droplets that seemingly must be overcome before coalescence can occur. Finally, case V sees a return of coalescence which is appreciably faster compared to case I. Even though the substrate patterns are very shallow, they are visually interesting: ridge heights are maximized at the loci where the residual ring patterns superimpose and intersect.

With that, we now turn our attention to droplet coalescence, since droplets are more experimentally observable compared to substrate deformations. Figure 6 shows that case I is characterized by late coalescence into a capsule shaped droplet, whereas case II is characterized by early coalescence into a stretched droplet, which eventually grows into a spherical one. Case III also tends towards early coalescence but the difference is that the resultant droplet is less stretched and eventually stick-slips into an asymmetric one. As for case IV, the droplets do not coalesce, as expected based on the substrate pattern behavior shown previously, except now we see the phenomenological evidence that the droplets are in fact separated for extended period of time. Finally, case V droplets grow and coalesce in an almost similar way as case I, except that the eventual coalesced droplet is spherical.

Between substrate and droplet profiles, the coalescence time appears to be non-linearly dependent on the damping characteristics of a viscoelastic substrate. This is a somewhat unintuitive result, since individual droplet has been shown to produce smoothly varying radial growth curves bridged only by a stick-slip intermediate regime (Fig. 3a). Instead, our results show that the substrate-droplet pairs interact significantly across viscoelastic timescales leading to non-linear coalescence outcomes, as exemplified by the protracted separation between droplets seen in case IV.

To quantify this result, we first define coalescence time t_c as the time when the contact lines defined by $h > 2h_e$ would intersect, and plot the normalized coalescence time $3Gt_c/2r_0$ against viscous damping $3G\mu_s h_e/4\gamma$ as shown in Fig. 7a. Starting from an under-damped coalescence time limit of 97.5, we find that the coalescence time first increases with increasing viscous damping, which we term as repulsion regime, and then decreases as coalescence occurs rapidly, which we term as attraction regime, before hitting a separation regime, where droplets remain separated over an indefinite period of time. With further increase in viscous damping, we find the droplets would coalesce once again, with a coalescence time that tends towards an over-damped coalescence time limit of 61.5. For comparison, one considers an adjacent pair of droplets with initial droplet radii r_0 and center-to-center half-length L_c on rigid, stiff surface limit with a contact time $t_c|_{r=L_c}$. To that, one can either read off Fig. 3(a) along $r = L_c = 5$, or solve equation (7), for a = 0.64 to arrive at a contact time $3Gt_c/2r_0$ of 67.6, which reasonably approximates the simulated coalescence time at the over-damped limit

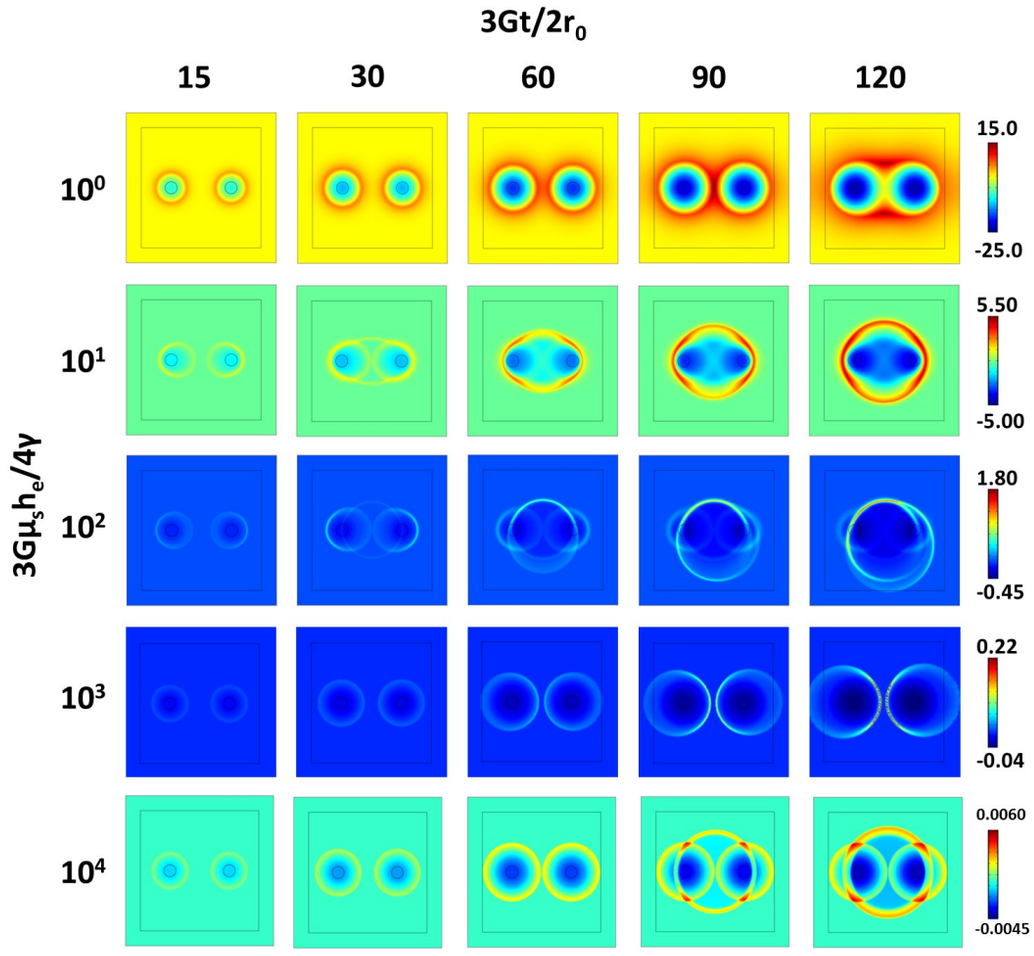

FIG. 5. Substrate height time-series (left to right) involving a pair of coalescing droplets each initialized as a hemispherical cap of radius $r_0 \equiv 10h_e$ growing at a constant rate G within a circle of radius r_0 centered $2L_c \equiv 10r_0$ from each other, shown in panels of size 250 by 250 and color-scaled to substrate height h_s. Substrate parameters are stiffness k_{ref} of 6.94×10^{-5} and tension γ_{ref} of 0.52, with viscous damping $3G\mu_s h_e/4\gamma$ shown in increasing order, from top to bottom (Cases I to V). Diverse substrate patterns emerge from coupled interactions between viscoelastic and growth timescales, as well as coalescence dynamics.

of 61.5.

The circle symbols shown on Fig. 7a indicate coalescence times for cases I, II, III and V, with case IV within the separation regime. To see how coalescence is stymied, we plot the evolution of substrate height for case IV in time as shown in Fig. 7b. Observe how the wetting ridges along the droplet centerline approach until a fixed distance before growing vertically upwards. The rate of upward growth $2r_0\partial_t h/3Gh_e$ is approximately constant so we can plot it against viscous damping $3G\mu_s h_e/4\gamma$ using modeling results obtained within the separation regime. The result is an inverse dependence as shown in inset of Fig. 7b, which suggests that an appropriate scaling for the growth rate of the wetting ridge is

$$\frac{\partial h}{\partial t} \sim \frac{2\gamma}{\mu_s r_0}, \tag{10}$$

which is independent of droplet growth rate.

When coalescence does occur, the onset of coalescence is characterized by the formation and growth of a capillary bridge between the droplets. For under-damped case I, we find a separation of time scales between the merging of substrate wetting ridge and the formation of liquid bridge as shown in Fig. 8(a,b). Since the deformation of the substrate is slow compared to the growth rate of the capillary bridge, the substrate height profile is essentially static at capillary timescales. In contrast, for over-damped case V, the coalescence and formation of bridge follows that of droplets on a rigid substrate.[45]

The apparent decoupling of time scales for under-damped case I suggests that the formation and growth of capillary bridge can be examined independently. Figure 9a shows that the capillary bridge height in post-coalescence time depends on the viscous damping, specifically, the under-damped growth (case I) is shown to level off quickly, whereas the over-damped growth (case V) persists. Rescaling to capillary time-

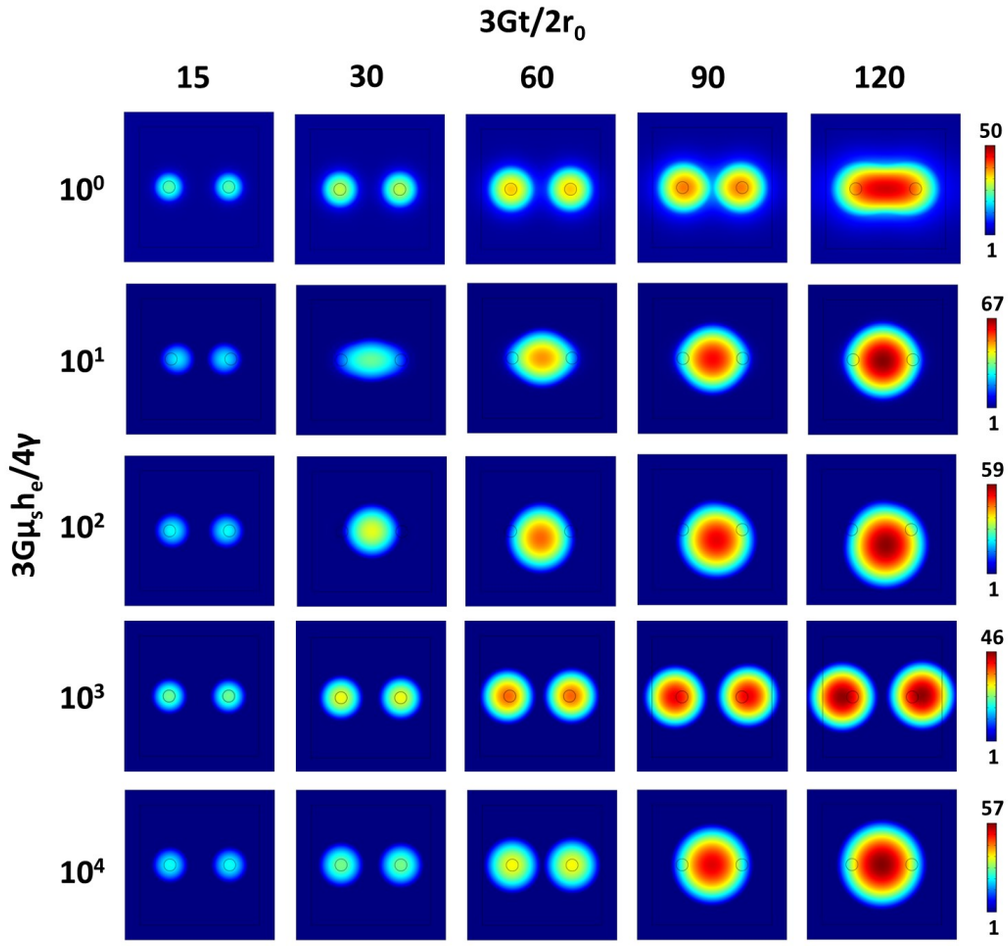

FIG. 6. Droplet height time-series (left to right) involving a pair of coalescing droplets each initialized as a hemispherical cap of radius $r_0 \equiv 10h_e$ growing at a constant rate G within a circle of radius r_0 centered $10r_0$ from each other, shown in panels of size 250 by 250 and color-scaled to height $(h+h_s)$. Substrate parameters are stiffness k_{ref} of 6.94×10^{-5} and tension γ_{ref} of 0.52, with viscous damping $3G\mu_s h_e/4\gamma$ shown in increasing order, top to bottom (cases I to V). Dynamic interactions between growing droplets and viscoelastic soft substrate yield nonlinear coalescence outcomes not observed for rigid substrate cases.

scales, Fig. 9b shows that the growth curves are linear at early times, corroborating a known scaling law for bridge height $h_c \sim (t-t_c)$ obtained by balancing Laplace pressure and viscous stress.[46]

V. CONCLUSIONS

We determined that liquid droplets interact with soft substrates across viscous time-scales leading to diverse outcomes. At intermediate viscous damping, an inflating droplet is shown to undergo stick-slip dynamics at the advancing wetting edge. Despite limitations in thin film approximation, our numerical simulations have accurately reproduced observations from published experimental results,[25] including a globular advancing front and a static rear, with no parameter adjustments. Significantly, when two adjacent droplets are inflated simultaneously, we found that differences in viscous damping could lead to non-linear coalescence outcomes, including attraction, repulsion and intriguingly, a separation regime, where growing droplets are prevented from coalescing over extended periods of time.

Here, we turn to an earlier study of water condensation on two cooled PDMS substrates, one more rigid than the other, under otherwise identical experimental conditions.[28] After four minutes, the droplets on the harder surface were observed to be predominantly spherical in shape, whereas those on the softer surface were, oddly enough, ellipsoidal. We note that our models show that the coalesced droplet is spherical for the over-damped case (case V), but ellipsoidal for the under-damped case (case I). The latter offers an explanation as to why isolated condensates were seen as ellipsoidal on soft substrates[28] – those are coalesced droplets.

On engineered surfaces, it is known that droplets spontaneously move on substrates with stiffness gradients[22] in a direction that also depends on wetting properties.[23] In re-

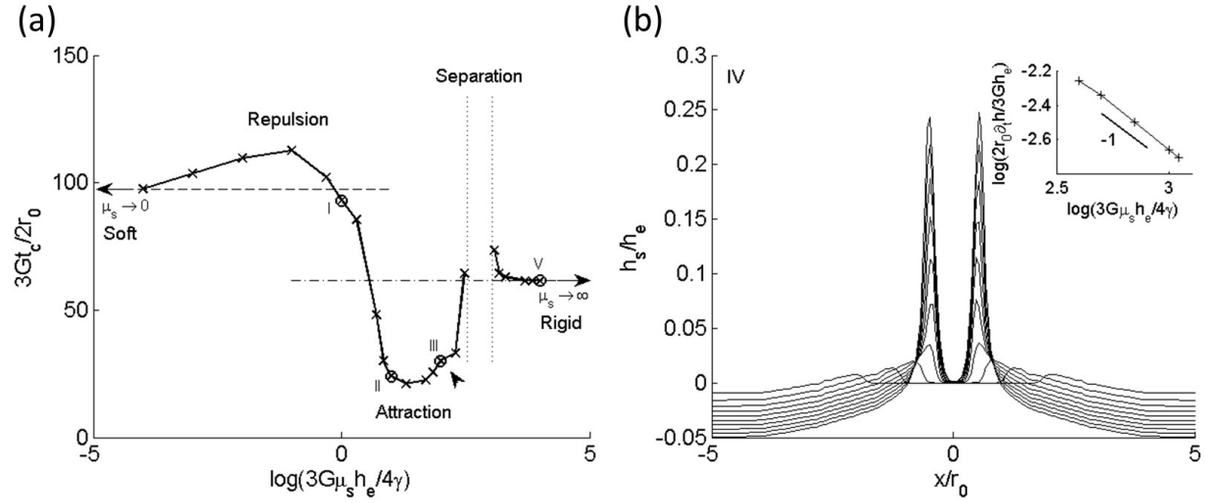

FIG. 7. (a) Plot of coalescence time $3Gt_c/2r_0$ against viscous damping $3G\mu_s h_e/4\gamma$ in semi-log scale reveals repulsion, attraction and separation regimes. Left arrow indicates under-damped soft limit ($\mu_s \to 0$) and right arrow indicates over-damped rigid limit ($\mu_s \to \infty$). Representative points (circle symbol) refer to cases I, II, III and V, and the arrow-head highlights to stick-slip regime. (b) Evolution of substrate height h_s/h_e along the center-line between separated droplets for case IV shows the attraction and growth of wetting ridges at a nearly constant rate. Inset shows logarithmic plot of the average growth rate of the ridge $2r_0\partial_t h/3Gh_e$ against the viscous damping $3G\mu_s h_e/4\gamma$, using only data points within the separation regime.

lated fields such as biology, we know that cells can preferentially migrate on soft substrates with stiffness gradients via durotaxis.[24] Although cells are known to gauge viscoelastic resistance to the traction force they apply on substrates,[47] it is not clear how cellular locomotion depends on the viscous damping component,[48,49] especially when contact guidance[50] is involved. We hope our study can inspire similar research based on dynamics of biological substrates including extracellular matrix.

Finally, we posit that dynamics of droplets on viscoelastic soft substrate will feature prominently in surface modification, either to prevent or to promote coalescence between condensates. Our study provides a roadmap for potential innovations in smart materials tuned for condensation control and self-cleaning applications.

CONFLICTS OF INTEREST

There are no conflicts to declare.

AUTHOR'S CONTRIBUTIONS

All authors contribute equally to this work.

ACKNOWLEDGEMENTS

This research is supported by A*STAR under Pharos "Advanced Surfaces" Program (Award 152 37 00103).

DATA AVAILABILITY STATEMENT

The data that support the findings of this study are available from the corresponding author upon reasonable request.

APPENDIX A: PARAMETER ESTIMATION

The model contains parameters which can be estimated using experimental fitting, namely, the substrate stiffness coefficient k_s and the solid-liquid interfacial tension γ_s. To that, we reference experimental data taken from Ref. 22 for two separate cases: a thin substrate case (14 μm), and a thick one (50 μm). We seek a fit in substrate height profile by optimizing both stiffness k_s and tension γ_s parameters. Since interfacial tension γ_s is independent of substrate thickness, we constrain the optimization so that the interfacial tension values are identical for both thick and thin substrate cases.

Fig. 10 shows the substrate height profiles for varying droplet sizes and their corresponding model fits using substrate stiffness k_s of 3.33 GPa/m for thin and 0.50 GPa/m for

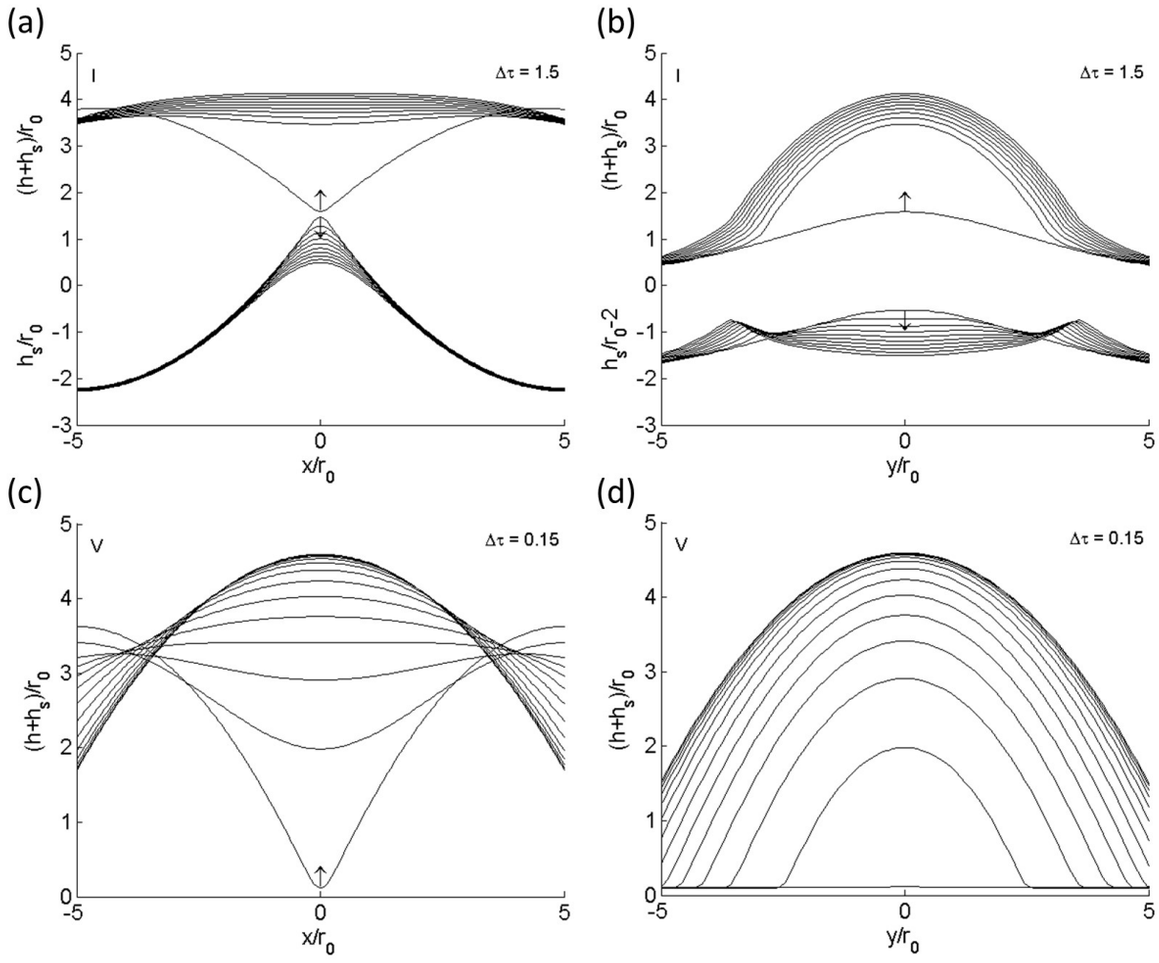

FIG. 8. (a,b) Evolution of liquid (upper) and substrate (lower) heights of the capillary bridge formed during coalescence for the under-damped case I, either aligned (a) or orthogonal (b) to the centerline between droplets, at frame interval $3G\Delta t/2r_0$ of 1.5 units. Substrate profile in (b) has been lowered by 2 units for clarity. (c,d) Evolution of liquid height of the capillary bridge formed during coalescence for the over-damped case V, either aligned (c) or orthogonal (d) to the centerline between droplets, at frame interval $3G\Delta t/2r_0$ of 0.15 units. Substrate heights are negligible in this case.

thick substrate cases, and interfacial tension γ_s of 0.0375 N/m for both. For static problems, the viscous damping coefficient μ_s is neglected. Comparison between the experimental and model substrate profiles for droplets of different radii show that both the modeled ridge height and substrate depth are in agreement, which is reasonable considering that only a two-parameter fit has been employed in a highly idealized substrate model. Still there are some discrepancies between the model fit and the experiment. For example, for small droplets on thin substrate, the substrate depression is under-estimated by the model, whereas for large droplets on thick substrate, the modeled depression is an over-estimate. In addition, the edges of the wetting ridge for thin substrates are convex, due to finite film thickness and material incompressibility.[51] These features cannot be captured by either a reduced model[52] or a one-dimensional Winkler's model[16], but they can be resolved by solving the full elastic equations for the substrate.[52]

This allows us to estimate characteristic values of substrate stiffness and tension of actual soft materials used in experiments. Based on the thick substrate case, we find substrate stiffness k_s = 0.50 GPa/m and interfacial tension γ_s = 0.0375 N/m, which translate to reference stiffness $k_{ref} \equiv k_s h_e^2/\gamma$ of 6.94×10^{-5} and reference tension $\gamma_{ref} \equiv \gamma_s/\gamma$ of 0.52.

APPENDIX B: SYMMETRY BREAKING AND MESHING

To show that asymmetric results (see Fig. 2) are physical and reproducible, simulations of stick-slip regime (Case III) are repeated with different mesh schemes, based on either advancing front or Delaunay tessellation. Mesh refinement is performed by limiting the maximum size of finite elements within a circle of radius $10r_0$ from the center. Numerical solvers are identical in all cases.

In the absence of external perturbations, the directions of droplet spreading and stick-slip growth depend only on nu-

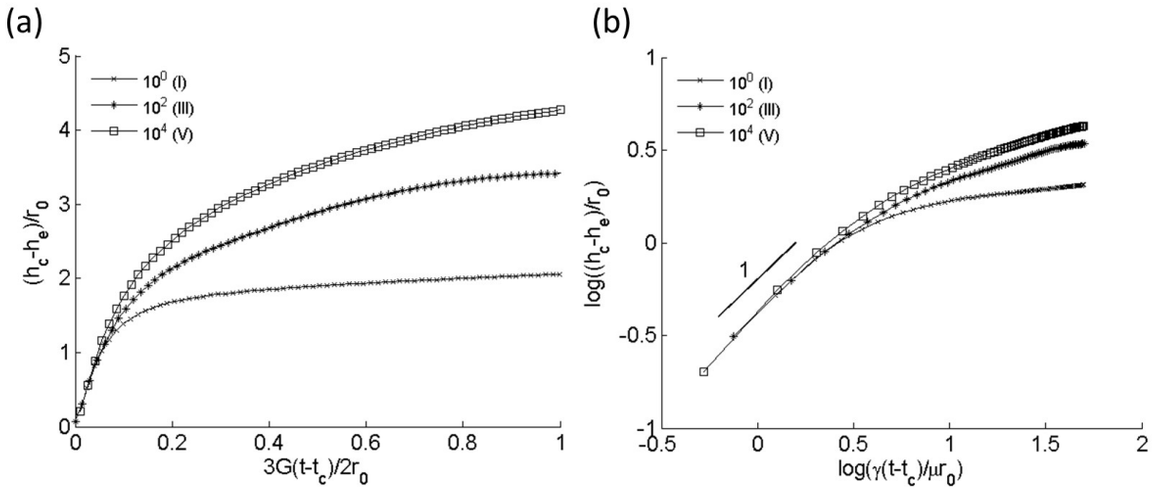

FIG. 9. Plots of capillary bridge height $(h_c - h_e)/r_0$ midpoint between coalescing droplets against time after contact $3G(t-t_c)/2r_0$ for select viscoelastic cases I, III and V. (b) Logarithmic plots of capillary bridge height $(h_c - h_e)/r_0$ against rescaled time $\gamma(t-t_c)/\mu r_0$ shows linear growth at early times, independent of viscous damping.

merical imperfections of the underlying mesh (Fig. 11). Asymmetric solutions are shown to be stable with increasing mesh resolutions.

[1]D. Bonn, J. Eggers, J. Indekeu, J. Meunier, and E. Rolley, "Wetting and spreading," Reviews of modern physics **81**, 739 (2009).
[2]L. Chen, E. Bonaccurso, T. Gambaryan-Roisman, V. Starov, N. Koursari, and Y. Zhao, "Static and dynamic wetting of soft substrates," Current opinion in colloid & interface science **36**, 46–57 (2018).
[3]J. Gerber, T. Lendenmann, H. Eghlidi, T. M. Schutzius, and D. Poulikakos, "Wetting transitions in droplet drying on soft materials," Nature communications **10**, 1–10 (2019).
[4]M. Napiórkowski, L. Schimmele, and S. Dietrich, "Wetting transitions on soft substrates," EPL (Europhysics Letters) **129**, 16002 (2020).
[5]H. Eral, J. Oh, *et al.*, "Contact angle hysteresis: a review of fundamentals and applications," Colloid and polymer science **291**, 247–260 (2013).
[6]B. Andreotti and J. H. Snoeijer, "Statics and dynamics of soft wetting," Annual Review of Fluid Mechanics **52** (2020).
[7]S. J. Park, B. M. Weon, J. San Lee, J. Lee, J. Kim, and J. H. Je, "Visualization of asymmetric wetting ridges on soft solids with x-ray microscopy," Nature communications **5**, 1–7 (2014).
[8]E. R. Jerison, Y. Xu, L. A. Wilen, and E. R. Dufresne, "Deformation of an elastic substrate by a three-phase contact line," Physical review letters **106**, 186103 (2011).
[9]G. Lester, "Contact angles of liquids at deformable solid surfaces," Journal of Colloid Science **16**, 315–326 (1961).
[10]R. W. Style and E. R. Dufresne, "Static wetting on deformable substrates, from liquids to soft solids," Soft Matter **8**, 7177–7184 (2012).
[11]R. D. Schulman and K. Dalnoki-Veress, "Liquid droplets on a highly deformable membrane," Physical review letters **115**, 206101 (2015).
[12]A. Marchand, S. Das, J. H. Snoeijer, and B. Andreotti, "Contact angles on a soft solid: From young's law to neumann's law," Physical review letters **109**, 236101 (2012).
[13]V. M. Starov and M. G. Velarde, *Wetting and spreading dynamics* (CRC press, 2019).
[14]B. Deryagin, V. Starov, and N. Churaev, "Pressure on a wetting perimeter," Colloid Journal of the USSR **44**, 770–775 (1982).
[15]P.-G. De Gennes, "Wetting: statics and dynamics," Reviews of modern physics **57**, 827 (1985).
[16]G. Ahmed, V. V. Kalinin, O. Arjmandi-Tash, and V. M. Starov, "Equilibrium of droplets on a deformable substrate: Influence of disjoining pressure," Colloids and Surfaces A: Physicochemical and Engineering Aspects **521**, 3–12 (2017).
[17]D. A. Dillard, B. Mukherjee, P. Karnal, R. C. Batra, and J. Frechette, "A review of winkler's foundation and its profound influence on adhesion and soft matter applications," Soft matter **14**, 3669–3683 (2018).
[18]G. Ahmed, N. Koursari, I. V. Kuchin, and V. M. Starov, "Hysteresis of contact angle of sessile droplets on deformable substrates: influence of disjoining pressure," Colloids and Surfaces A: Physicochemical and Engineering Aspects **546**, 129–135 (2018).
[19]M. Gielok, M. Lopes, E. Bonaccurso, and T. Gambaryan-Roisman, "Droplet on an elastic substrate: Finite element method coupled with lubrication approximation," Colloids and Surfaces A: Physicochemical and Engineering Aspects **521**, 13–21 (2017).
[20]R. W. Style, A. Jagota, C.-Y. Hui, and E. R. Dufresne, "Elastocapillarity: Surface tension and the mechanics of soft solids," Annual Review of Condensed Matter Physics **8**, 99–118 (2017).
[21]B. Andreotti and J. H. Snoeijer, "Soft wetting and the shuttleworth effect, at the crossroads between thermodynamics and mechanics," EPL (Europhysics Letters) **113**, 66001 (2016).
[22]R. W. Style, Y. Che, S. J. Park, B. M. Weon, J. H. Je, C. Hyland, G. K. German, M. P. Power, L. A. Wilen, J. S. Wettlaufer, *et al.*, "Patterning droplets with durotaxis," Proceedings of the National Academy of Sciences **110**, 12541–12544 (2013).
[23]J. Bueno, Y. Bazilevs, R. Juanes, and H. Gomez, "Wettability control of droplet durotaxis," Soft matter **14**, 1417–1426 (2018).
[24]C.-M. Lo, H.-B. Wang, M. Dembo, and Y.-l. Wang, "Cell movement is guided by the rigidity of the substrate," Biophysical journal **79**, 144–152 (2000).
[25]T. Kajiya, A. Daerr, T. Narita, L. Royon, F. Lequeux, and L. Limat, "Advancing liquid contact line on visco-elastic gel substrates: stick-slip vs. continuous motions," Soft Matter **9**, 454–461 (2013).
[26]T. Kajiya, P. Brunet, A. Daerr, L. Royon, T. Narita, F. Lequeux, and L. Limat, "Wetting on gels: Howthe gel characteristics affect the contact line dynamics," Interfacial Phenomena and Heat Transfer **1** (2013).
[27]T. Kajiya, P. Brunet, L. Royon, A. Daerr, M. Receveur, and L. Limat, "A liquid contact line receding on a soft gel surface: dip-coating geometry investigation," Soft Matter **10**, 8888–8895 (2014).

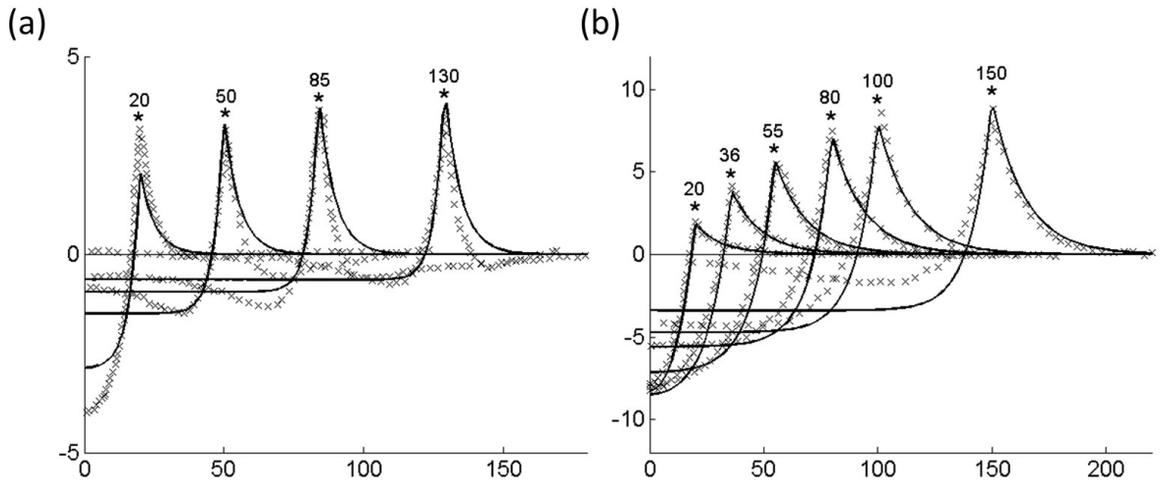

FIG. 10. Substrate profiles for varying droplet radii comparing experimental data (symbol) sampled from Ref.[22] and model fittings (line), based on (a) thin substrate ($14\mu m$) using substrate stiffness k_s of 3.33 GPa/m, and (b) thick substrate ($50\mu m$) using k_s of 0.50 GPa/m, and substrate tension γ_s of $0.0375N/m$ for both. Liquid surface tension γ is $0.072N/m$, dynamic viscosity μ is 0.001 $Pa \cdot s$, equilibrium film thickness h_e is 0.1 μm, disjoining pressure coefficient Π_0 is 5.0 MPa and viscous damping coefficient μ_s is neglected. Figure dimensions are in microns.

[28]M. Sokuler, G. K. Auernhammer, M. Roth, C. Liu, E. Bonacurrso, and H.-J. Butt, "The softer the better: fast condensation on soft surfaces," Langmuir **26**, 1544–1547 (2010).
[29]J. Eggers, J. R. Lister, and H. A. Stone, "Coalescence of liquid drops," Journal of Fluid Mechanics **401**, 293–310 (1999).
[30]D. G. Aarts, H. N. Lekkerkerker, H. Guo, G. H. Wegdam, and D. Bonn, "Hydrodynamics of droplet coalescence," Physical review letters **95**, 164503 (2005).
[31]R. Narhe, D. Beysens, and V. Nikolayev, "Contact line dynamics in drop coalescence and spreading," Langmuir **20**, 1213–1221 (2004).
[32]J. Hernández-Sánchez, L. Lubbers, A. Eddi, and J. Snoeijer, "Symmetric and asymmetric coalescence of drops on a substrate," Physical review letters **109**, 184502 (2012).
[33]S. Karpitschka, C. Hanske, A. Fery, and H. Riegler, "Coalescence and noncoalescence of sessile drops: impact of surface forces," Langmuir **30**, 6826–6830 (2014).
[34]H. P. Kavehpour, "Coalescence of drops," Annual Review of Fluid Mechanics **47**, 245–268 (2015).
[35]S. Karpitschka, A. Pandey, L. A. Lubbers, J. H. Weijs, L. Botto, S. Das, B. Andreotti, and J. H. Snoeijer, "Liquid drops attract or repel by the inverted cheerios effect," Proceedings of the National Academy of Sciences **113**, 7403–7407 (2016).
[36]D. Vella and L. Mahadevan, "The "cheerios effect"," American journal of physics **73**, 817–825 (2005).
[37]L. Cacopardo, N. Guazzelli, R. Nossa, G. Mattei, and A. Ahluwalia, "Engineering hydrogel viscoelasticity," Journal of the mechanical behavior of biomedical materials **89**, 162–167 (2019).
[38]A. Oron, S. H. Davis, and S. G. Bankoff, "Long-scale evolution of thin liquid films," Reviews of modern physics **69**, 931 (1997).
[39]L. W. Schwartz and R. R. Eley, "Simulation of droplet motion on low-energy and heterogeneous surfaces," Journal of Colloid and Interface Science **202**, 173–188 (1998).
[40]N. Koursari, G. Ahmed, and V. M. Starov, "Equilibrium droplets on deformable substrates: Equilibrium conditions," Langmuir **34**, 5672–5677 (2018).
[41]N. H. Mostafa, "Effect of a viscoelastic foundation on the dynamic stability of a fluid conveying pipe," International Journal of Applied Science and Engineering **12**, 59–74 (2014).
[42]N. Savva and S. Kalliadasis, "Dynamics of moving contact lines: A comparison between slip and precursor film models," EPL (Europhysics Letters) **94**, 64004 (2011).
[43]D. Beysens, "Dew nucleation and growth," Comptes Rendus Physique **7**, 1082–1100 (2006).
[44]T. Rogers, K. Elder, and R. C. Desai, "Droplet growth and coarsening during heterogeneous vapor condensation," Physical Review A **38**, 5303 (1988).
[45]W. Ristenpart, P. McCalla, R. Roy, and H. A. Stone, "Coalescence of spreading droplets on a wettable substrate," Physical review letters **97**, 064501 (2006).
[46]R. Narhe, D. Beysens, and Y. Pomeau, "Dynamic drying in the early-stage coalescence of droplets sitting on a plate," EPL (Europhysics Letters) **81**, 46002 (2008).
[47]O. Chaudhuri, L. Gu, M. Darnell, D. Klumpers, S. A. Bencherif, J. C. Weaver, N. Huebsch, and D. J. Mooney, "Substrate stress relaxation regulates cell spreading," Nature communications **6**, 1–7 (2015).
[48]M. Bennett, M. Cantini, J. Reboud, J. M. Cooper, P. Roca-Cusachs, and M. Salmeron-Sanchez, "Molecular clutch drives cell response to surface viscosity," Proceedings of the National Academy of Sciences **115**, 1192–1197 (2018).
[49]K. Dey, S. Agnelli, and L. Sartore, "Dynamic freedom: substrate stress relaxation stimulates cell responses," Biomaterials science **7**, 836–842 (2019).
[50]J. Feng, H. Levine, X. Mao, and L. M. Sander, "Cell motility, contact guidance, and durotaxis," Soft matter **15**, 4856–4864 (2019).
[51]R. Pericet-Camara, G. K. Auernhammer, K. Koynov, S. Lorenzoni, R. Raiteri, and E. Bonaccurso, "Solid-supported thin elastomer films deformed by microdrops," Soft Matter **5**, 3611–3617 (2009).
[52]A. I. Rusanov, "Theory of wetting of elastically deformed bodies. 1. deformation with a finite contact-angle," Colloid Journal of the USSR **37**, 614–622 (1975).
[53]J. B. Bostwick, M. Shearer, and K. E. Daniels, "Elastocapillary deformations on partially-wetting substrates: rival contact-line models," Soft Matter

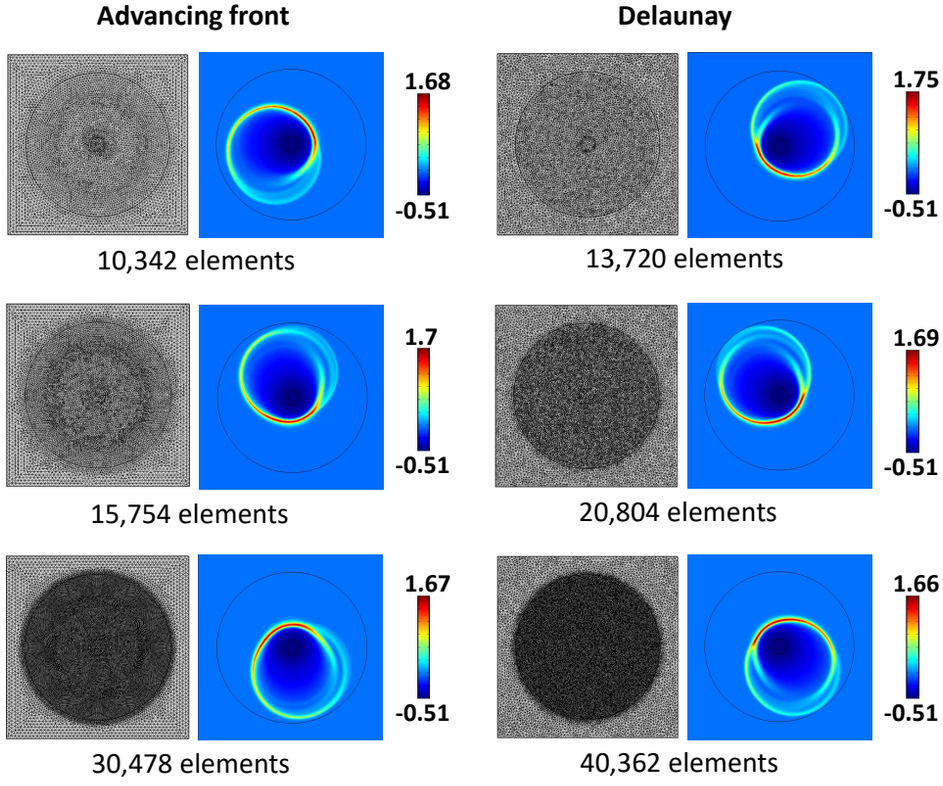

FIG. 11. Simulations of a Case III droplet (Fig. 2) repeated with different mesh schemes, based on either advancing front (left column) or Delaunay (right column) tessellation. Colored panels indicate scaled substrate height. Asymmetric solutions are shown to be reproducible and stable with increasing mesh resolutions.

10, 7361–7369 (2014).

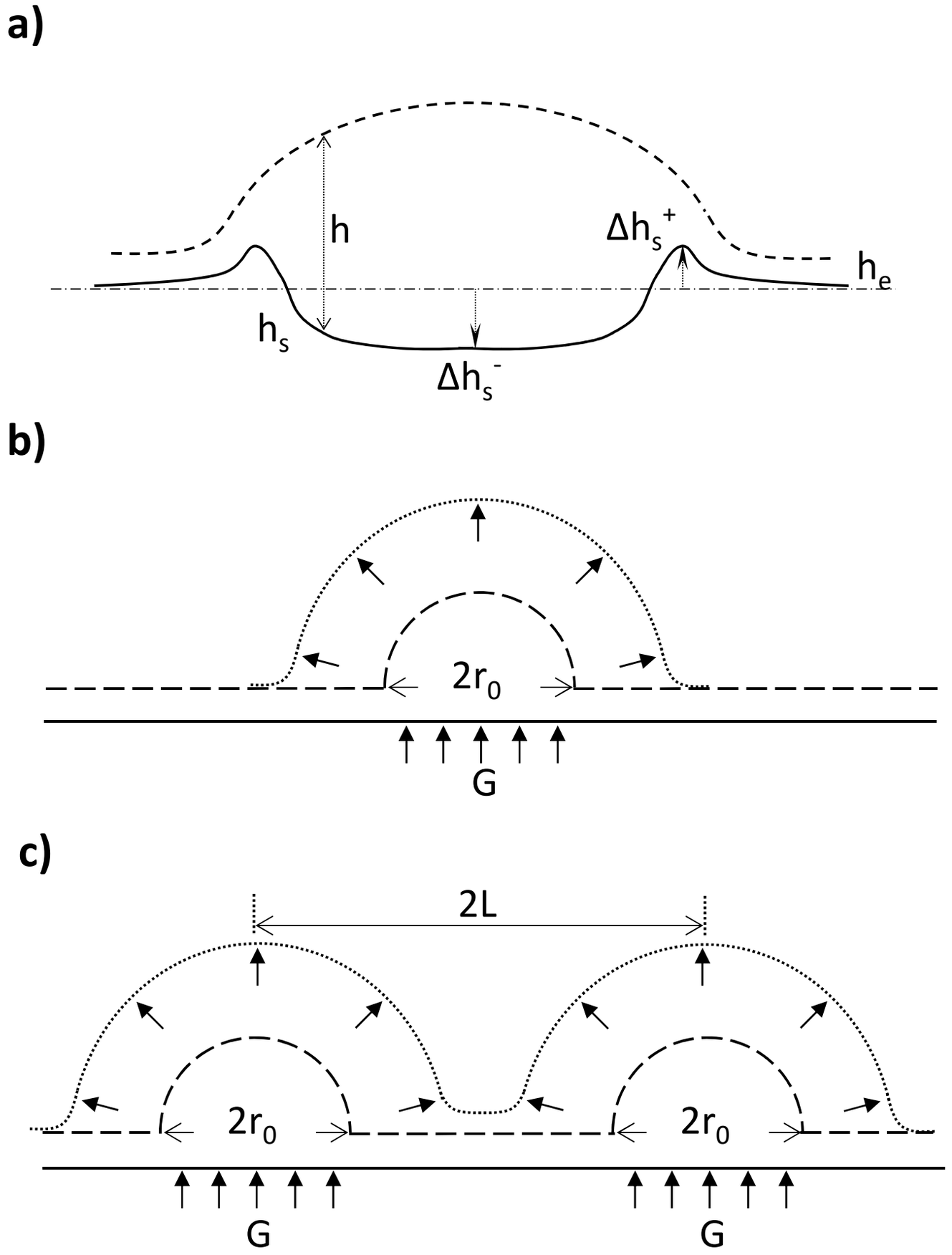

Case	$3G\mu_s h_e/4\gamma$	Droplet	Substrate	Characteristics
I	10^0	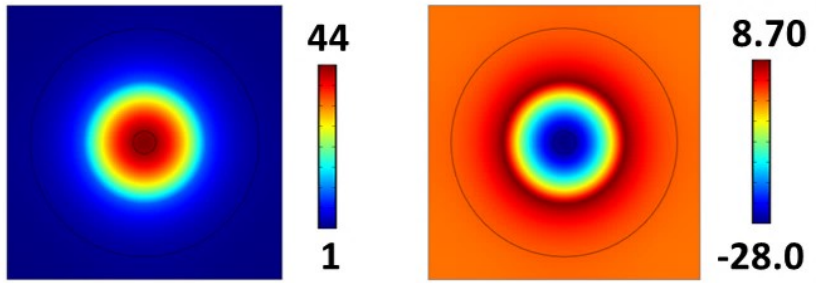		Symmetric, smooth
II	10^1	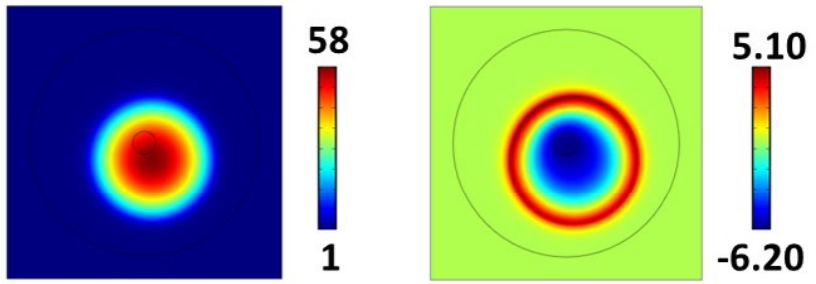		Asymmetric, smooth
III	10^2	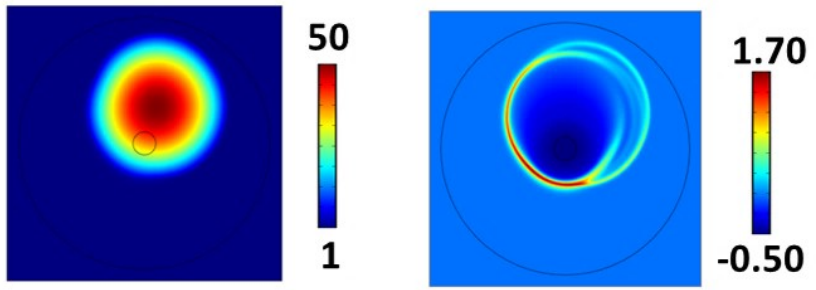		Asymmetric, stick-slip, irregular
IV	10^3	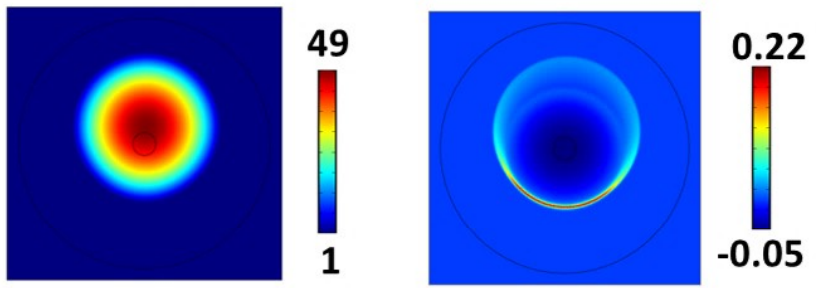		Asymmetric, stick-slip, regular
V	10^4	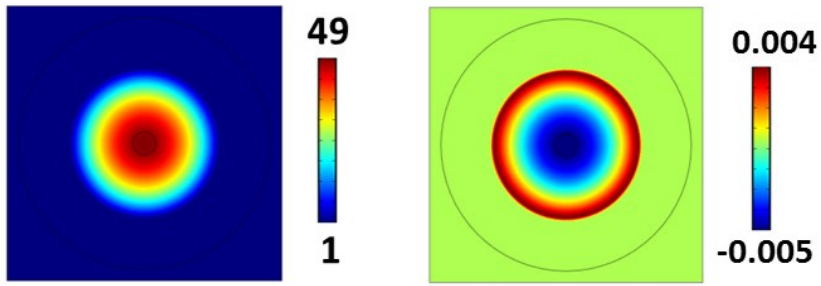		Symmetric, smooth, shallow

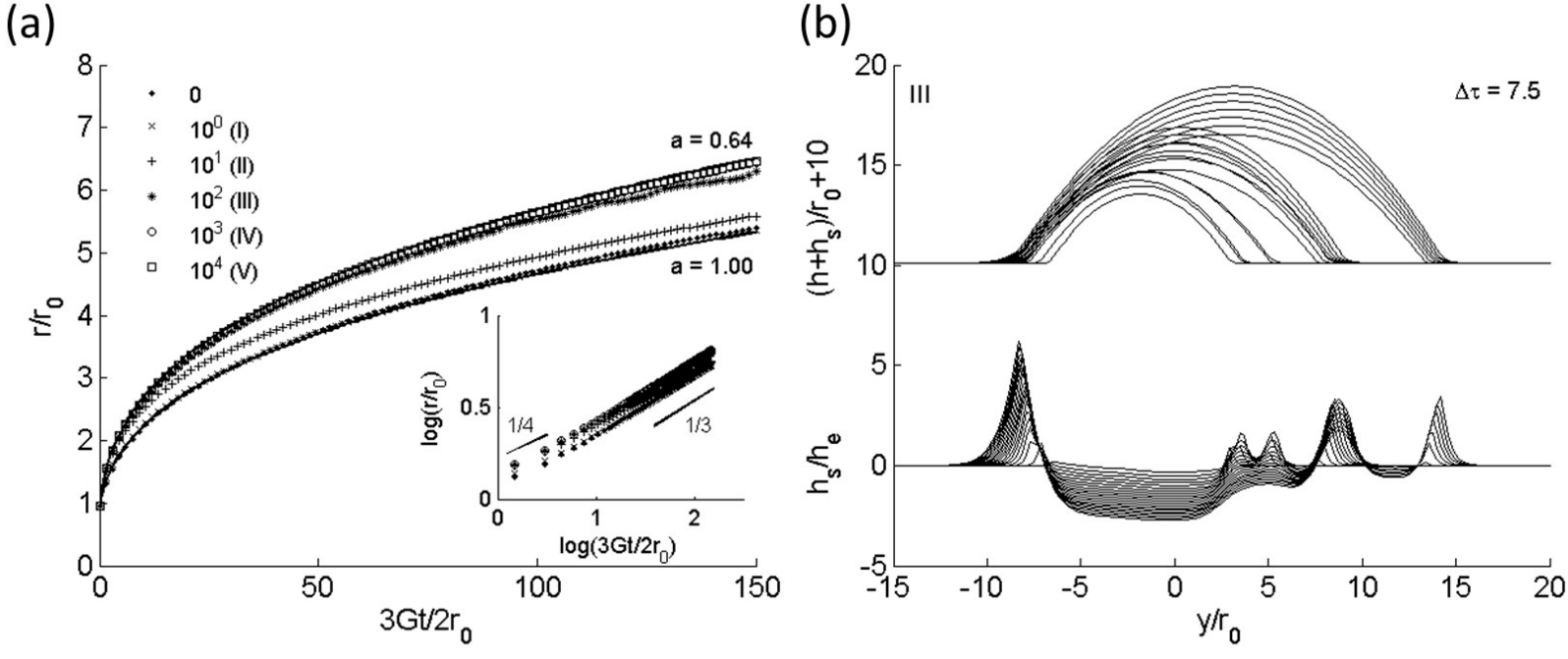
(a)
0
10^0 (I)
10^1 (II)
10^2 (III)
10^3 (IV)
10^4 (V)
a = 0.64
a = 1.00
r/r_0
3Gt/2r_0
log(r/r_0)
log(3Gt/2r_0)
1/4
1/3
(b)
III
Δτ = 7.5
(h+h_s)/r_0+10
h_s/h_e
y/r_0

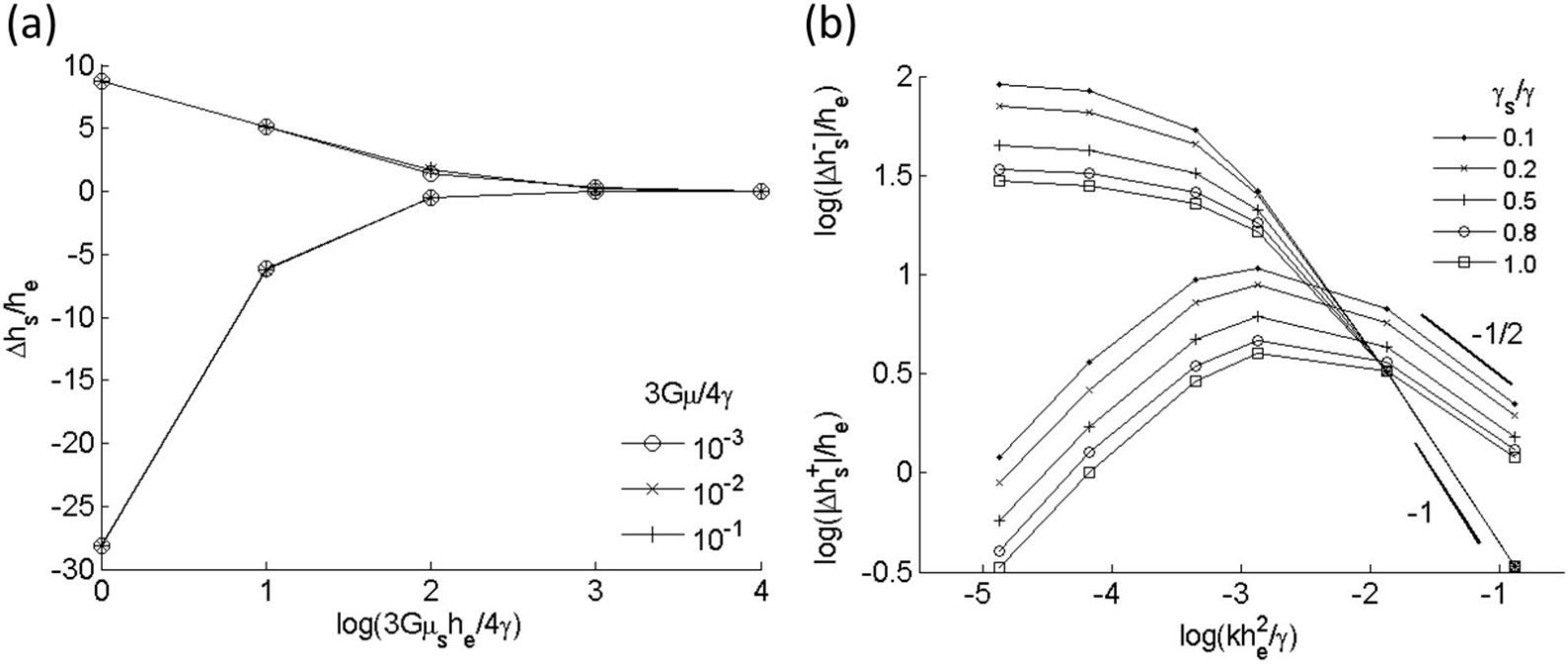
(a)
10
5
0
-5
-10
-15
-20
-25
-30
0
1
2
3
4
$\Delta h_s/h_e$
$\log(3G\mu_s h_e/4\gamma)$
$3G\mu/4\gamma$
10^{-3}
10^{-2}
10^{-1}
(b)
2
1.5
1
0.5
0
-0.5
-5
-4
-3
-2
-1
$\log(|\Delta h_s^-|/h_e)$
$\log(|\Delta h_s^+|/h_e)$
$\log(kh_e^2/\gamma)$
γ_s/γ
0.1
0.2
0.5
0.8
1.0
-1/2
-1

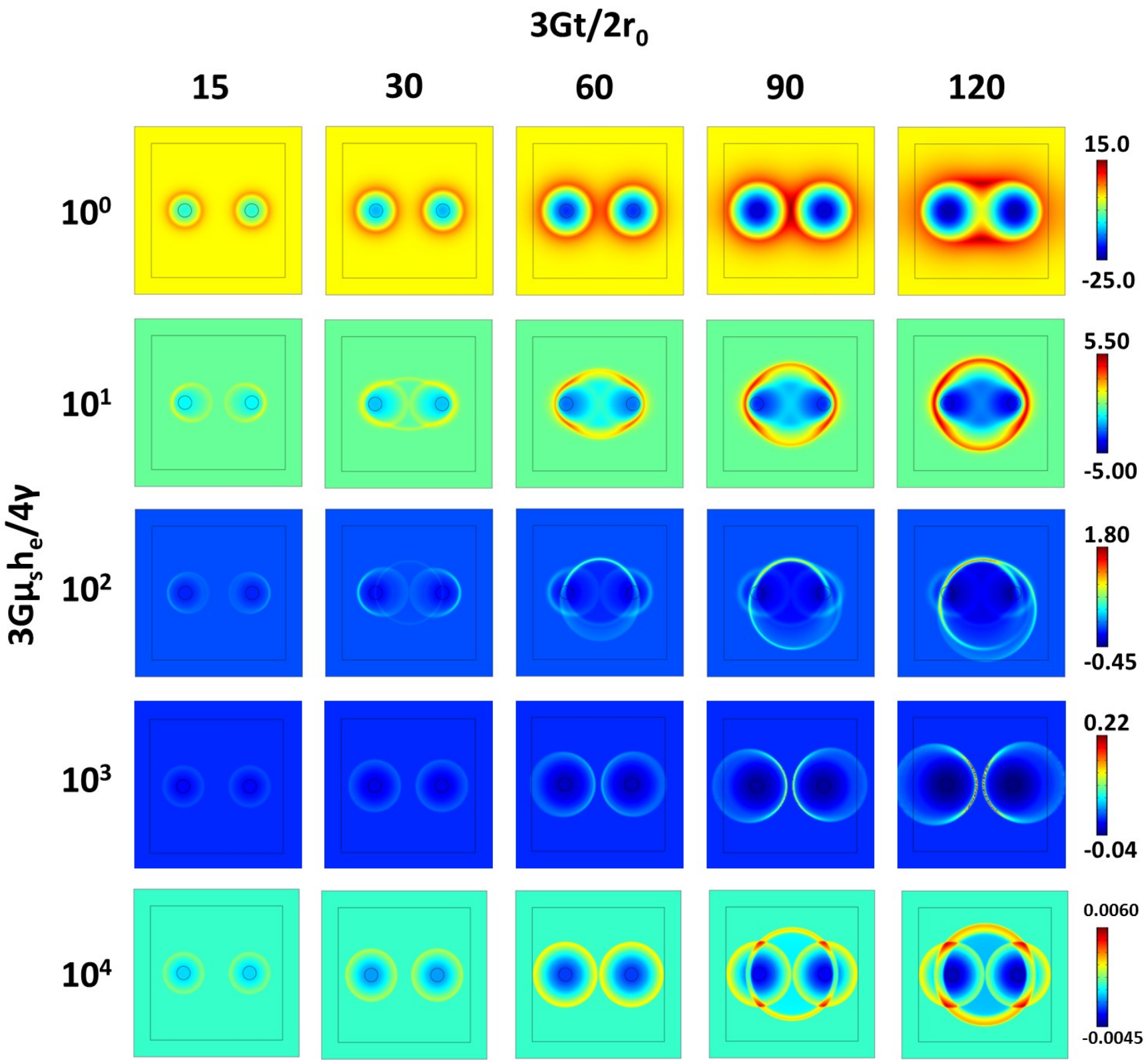
3Gt/2r0
15
30
60
90
120
3Gμshe/4γ
10^0
10^1
10^2
10^3
10^4
15.0
-25.0
5.50
-5.00
1.80
-0.45
0.22
-0.04
0.0060
-0.0045

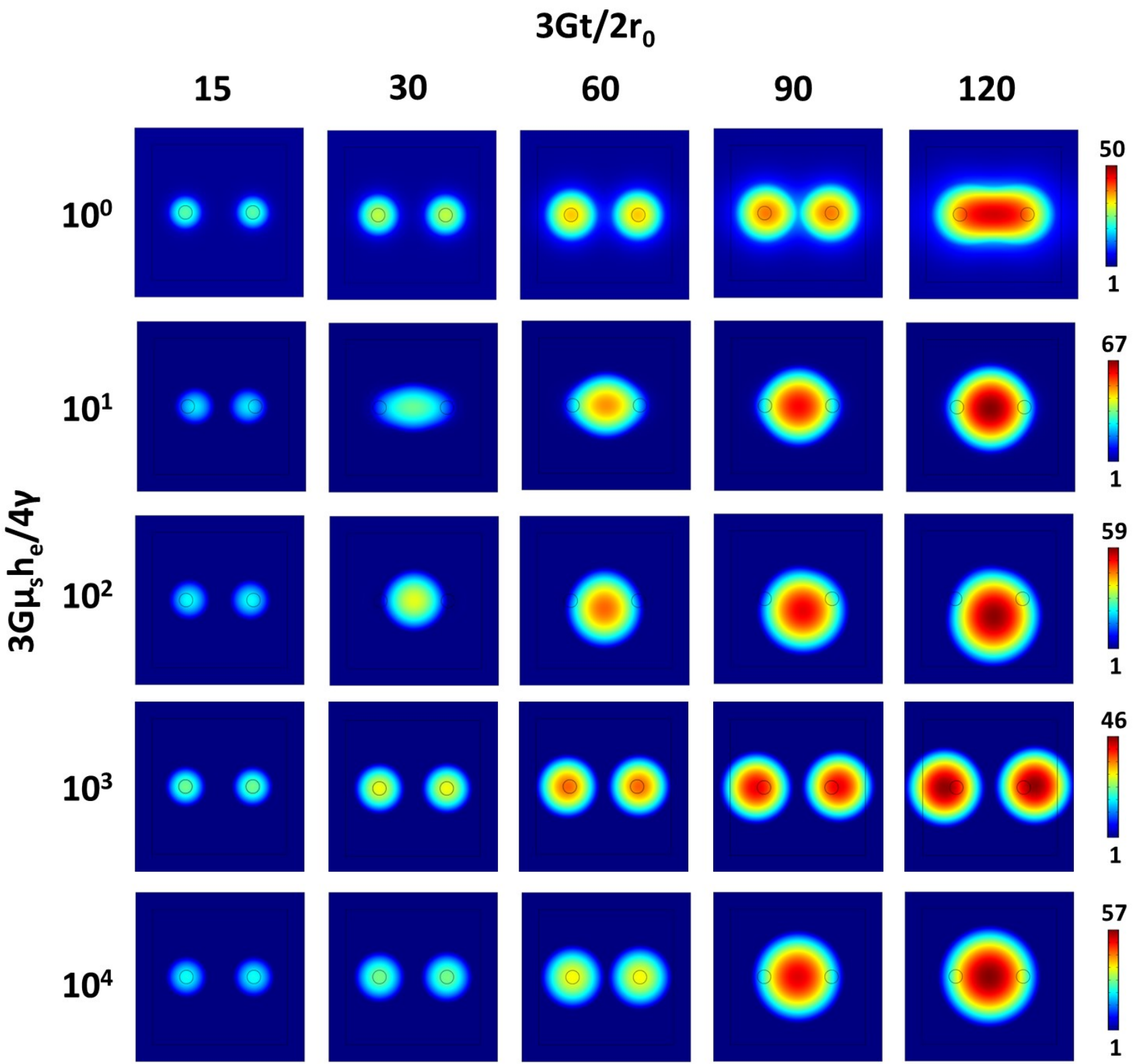
3Gt/2r0
15
30
60
90
120
3Gμshe/4γ
10^0
10^1
10^2
10^3
10^4
50
1
67
1
59
1
46
1
57
1

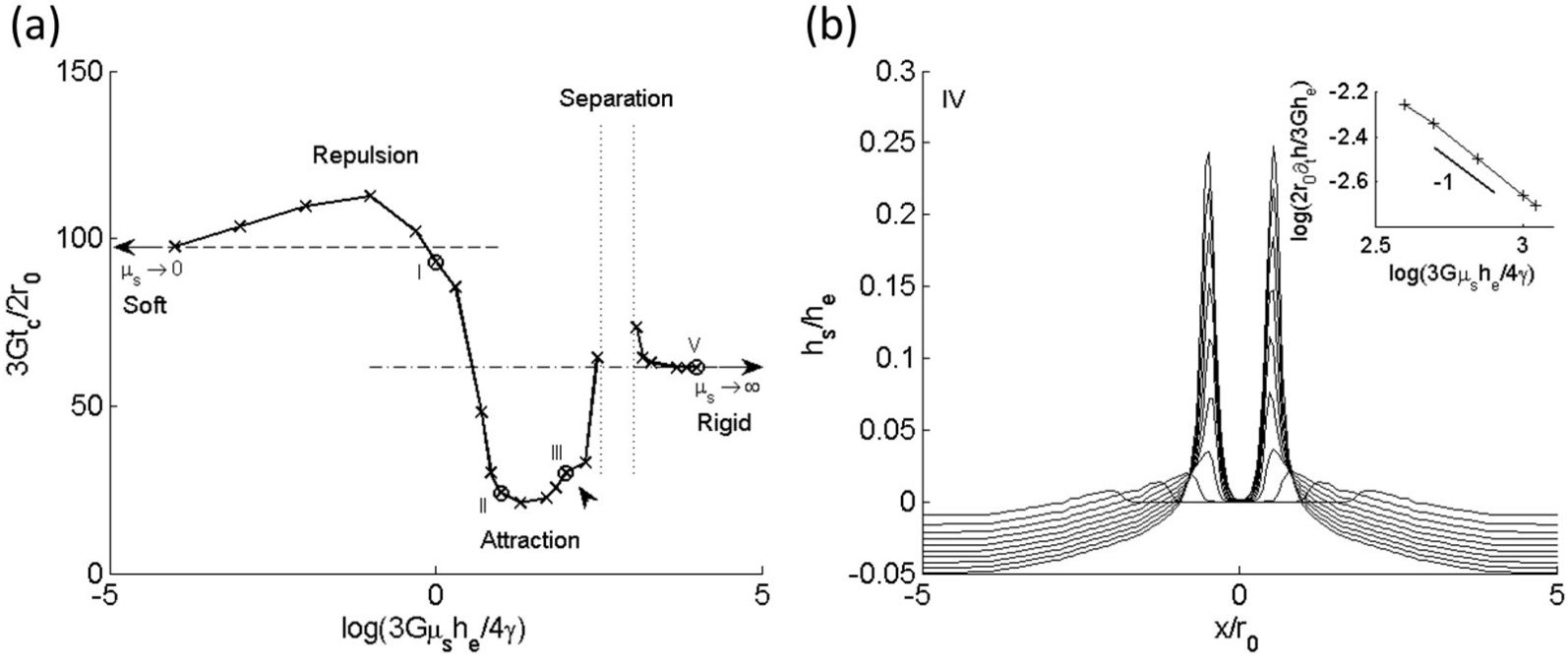
(a)
150
100
50
0
-5
0
5
$3Gt_c/2r_0$
$\log(3G\mu_s h_e/4\gamma)$
Separation
Repulsion
$\mu_s \to 0$
Soft
I
II
III
Attraction
V
$\mu_s \to \infty$
Rigid
(b)
0.3
0.25
0.2
0.15
0.1
0.05
0
-0.05
-5
0
5
h_s/h_e
x/r_0
IV
-2.2
-2.4
-2.6
2.5
3
-1
$\log(2r_0\dot{\varepsilon}_t h/3Gh_e)$
$\log(3G\mu_s h_e/4\gamma)$

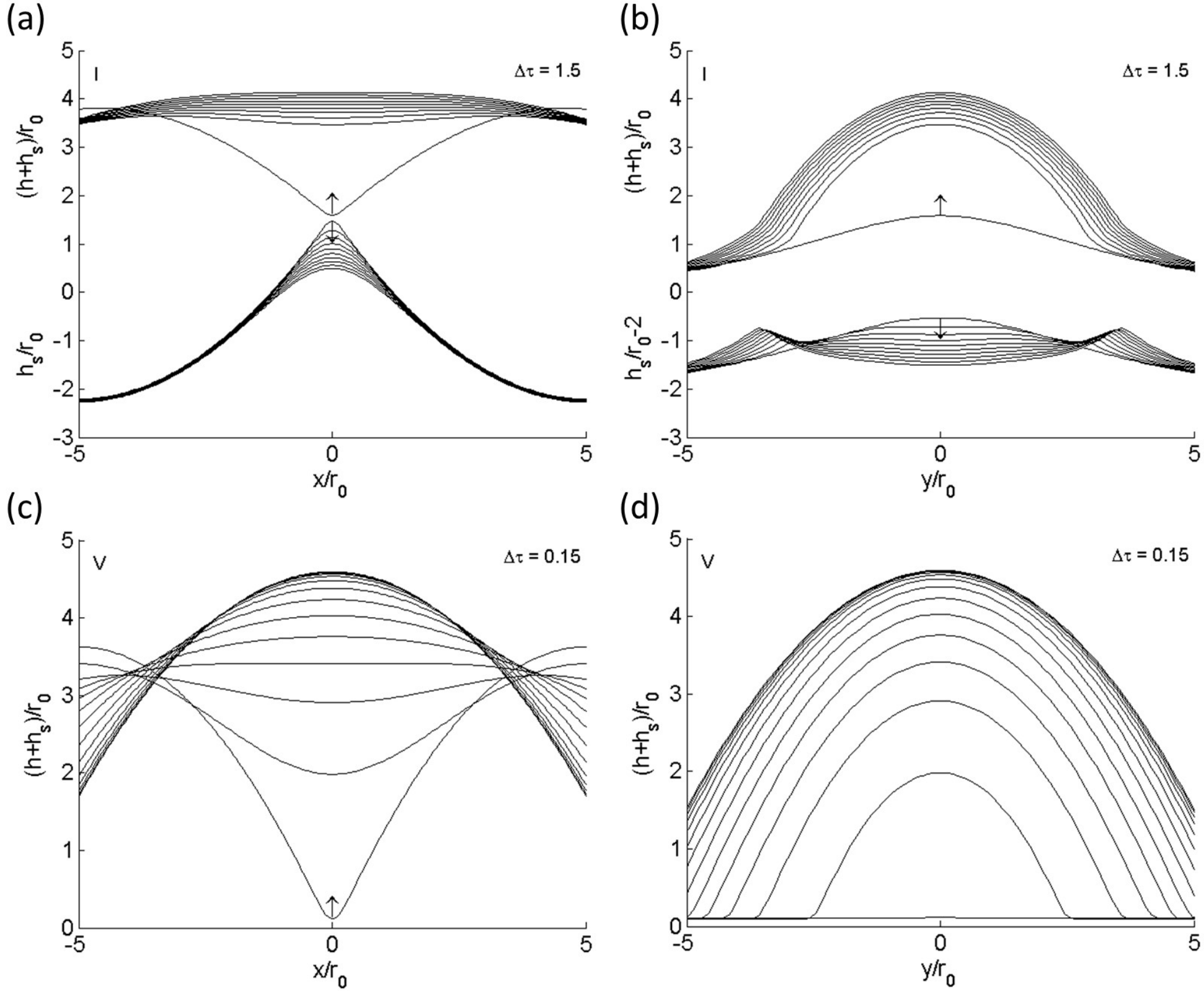
(a)
I
Δτ = 1.5
(h+h_s)/r_0
h_s/r_0
x/r_0
(b)
I
Δτ = 1.5
(h+h_s)/r_0
h_s/r_0^-2
y/r_0
(c)
V
Δτ = 0.15
(h+h_s)/r_0
x/r_0
(d)
V
Δτ = 0.15
(h+h_s)/r_0
y/r_0

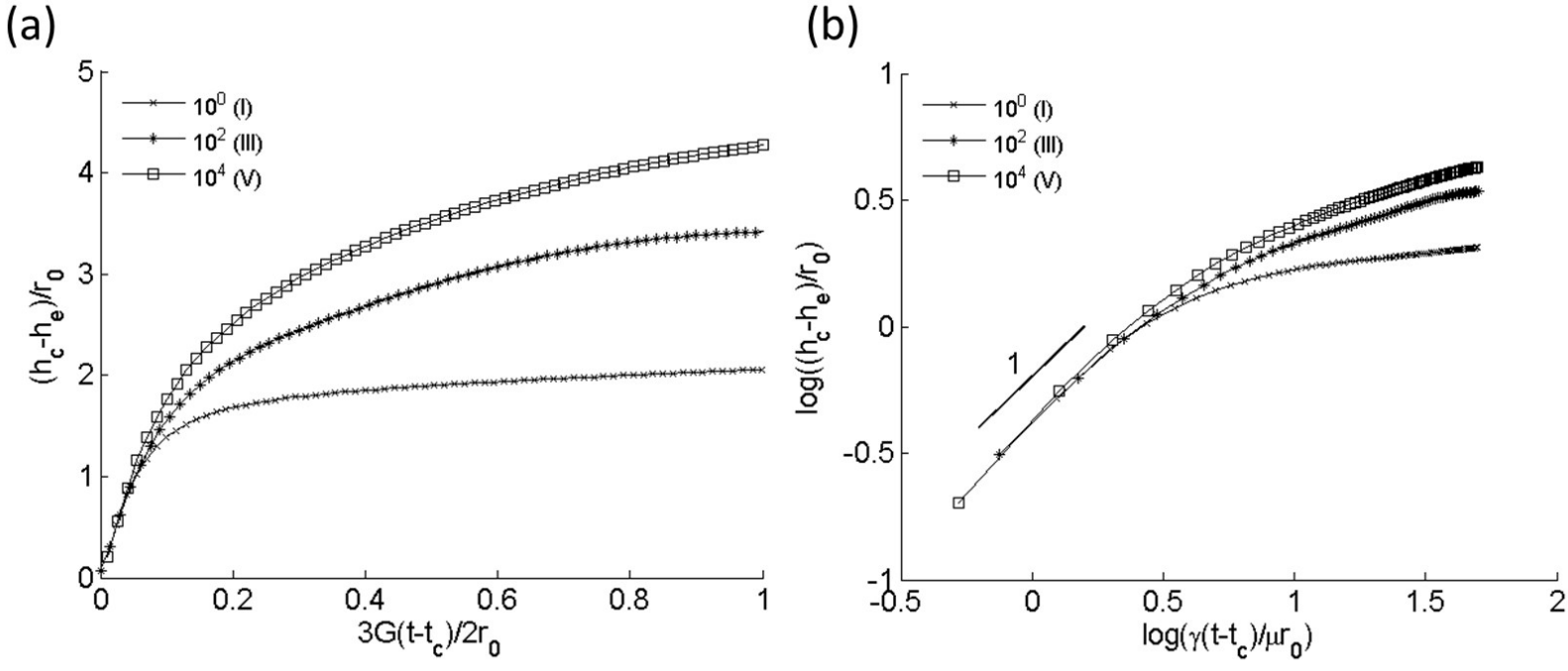
(a)
(b)
10^0 (I)
10^2 (III)
10^4 (V)
$(h_c-h_e)/r_0$
$3G(t-t_c)/2r_0$
$\log((h_c-h_e)/r_0)$
$\log(\gamma(t-t_c)/\mu r_0)$
1

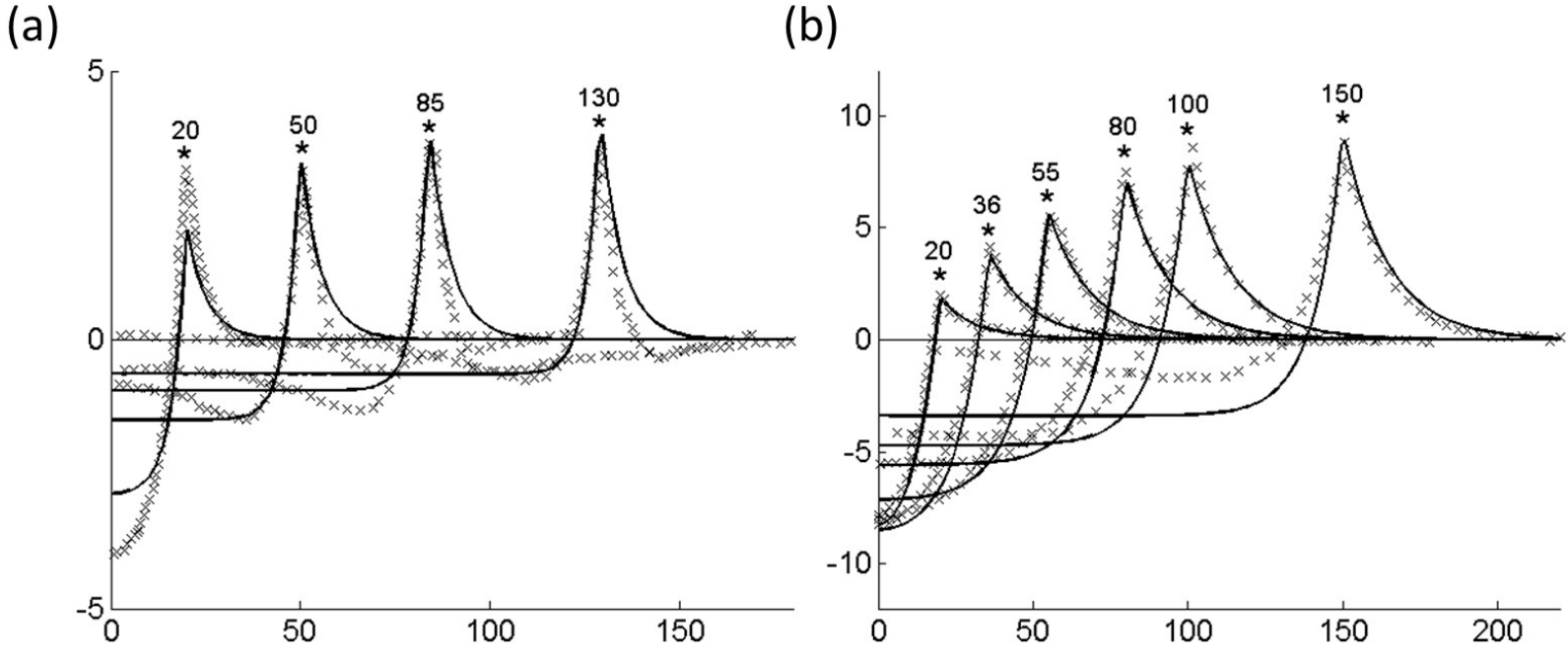
(a)
5
0
-5
0
50
100
150
20
50
85
130
(b)
10
5
0
-5
-10
0
50
100
150
200
20
36
55
80
100
150

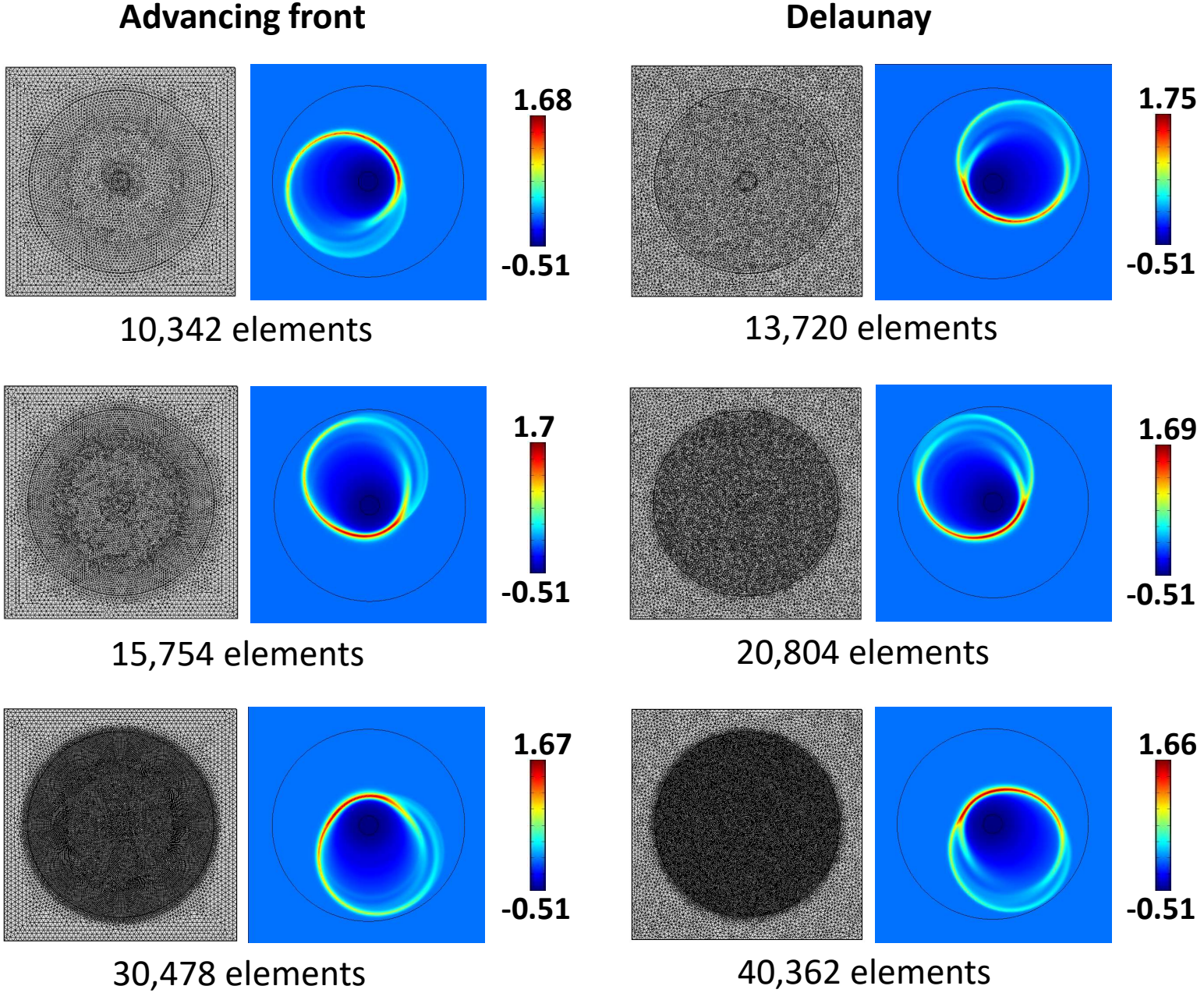
Advancing front
Delaunay
1.68
-0.51
1.75
-0.51
10,342 elements
13,720 elements
1.7
-0.51
1.69
-0.51
15,754 elements
20,804 elements
1.67
-0.51
1.66
-0.51
30,478 elements
40,362 elements